coatings

MDPI

Review

Tribology of 2D Nanomaterials: A Review

Paul C. Uzoma [1,2], Huan Hu [1], Mahdi Khadem [3] and Oleksiy V. Penkov [1,*]

[1] ZJU-UIUC Institute, International Campus, Zhejiang University, Jiaxing 314400, China; pauluzoma@futo.edu.ng (P.C.U.); huanhu@intl.zju.edu.cn (H.H.)
[2] Department of Polymer and Textile Engineering, Federal University of Technology, P.M.B. 1526, Owerri 460114, Nigeria
[3] Department of Mechanical Engineering, Yonsei University, Seoul 03722, Korea; mehdi.skyline@yonsei.ac.kr
* Correspondence: oleksiypenkov@intl.zju.edu.cn

Received: 29 August 2020; Accepted: 16 September 2020; Published: 18 September 2020

Abstract: The exfoliation of graphene has opened a new frontier in material science with a focus on 2D materials. The unique thermal, physical and chemical properties of these materials have made them one of the choicest candidates in novel mechanical and nano-electronic devices. Notably, 2D materials such as graphene, MoS_2, WS_2, h-BN and black phosphorus have shown outstanding lowest frictional coefficients and wear rates, making them attractive materials for high-performance nano-lubricants and lubricating applications. The objective of this work is to provide a comprehensive overview of the most recent developments in the tribological potentials of 2D materials. At first, the essential physical, wear and frictional characteristics of the 2D materials including their production techniques are discussed. Subsequently, the experimental explorations and theoretical simulations of the most common 2D materials are reviewed in regards to their tribological applications such as their use as solid lubricants and surface lubricant nano-additives. The effects of micro/nano textures on friction behavior are also reviewed. Finally, the current challenges in tribological applications of 2D materials and their prospects are discussed.

Keywords: friction; wear; 2D nanomaterials; tribology

1. Introduction

Containing friction and wear is a global problem because it is connected to an expanded range of material applications from simple tools to industrial machine components, medical devices, microelectrochemical systems (MEMS) and nanoelectromechanical systems (NEMS). The estimated world's total energy consumption emanating from tribological contacts is ~23% (119 EJ) [1]. From that, 20% (103 EJ) is employed to overcome friction and 3% (16 EJ) is utilized to reproduce worn parts and spare equipment caused by wear and wear-related failures. It is estimated that, if the world takes advantage of the available technologies targeted at improving tribological performance, the energy losses as a result of friction and wear could potentially be decreased by 40% and 18% in the short and long term, respectively. Globally, this would lead to 1.4% of GDP annually and 8.7% of the total energy consumption in the long term. Moreover, in the short term, it can decrease the global CO_2 emissions by as high as 1460 $MtCO_2$ leading to €450,000 million. The decrease could be 3140 $MtCO_2$ and the cost savings €970,000 million in the long term [1–3]. These observations have led to a concerted global effort, and substantial scientific interests in developing new technologies are focused on the reduction of friction and improved wear resistance.

Lubrication is generally recognized as the most effective way to control friction and wear; hence, extensive research is ongoing to develop a high-performance lubricant. Currently, the most common lubricants are fundamentally composed of base oil and an additive, which determines their overall performance. The major components of the lubricant determine its primary behavior, while the

additives play a vital role in impacting new properties or making up for the disadvantages in the base oil [4]. So, the need for a high-performance lubricant additive has greatly increased. Furthermore, tribological behavior is very vital in the overall performance of MEMS and NEMS, such as gears, switches and actuators. Since these systems are very small, they possess tight tolerance, so the effectiveness of the mechanical components largely depends on their frictional properties, and their commercial essence depends on their wear resistance [5]. The conventional liquid lubricants cannot be used in MEMS and NEMS due to the effect of surface tension; therefore, solid lubricants are required to achieve excellent friction and wear under dry conditions in these microdevices.

Two-dimensional layered-structured materials like graphene have over the decade attracted colossal interest as solid lubricants and lubrication nano-additives due to their excellent tribological performance originating from their unique chemical and physical properties. Geim and Novoslov were the first to introduce the "Scotch-tape-Method", which is an efficient way to produce comparatively large isolated graphene nanosheet samples [6–8]. Subsequently, researchers across the globe have extensively studied and reported on new classes of 2D materials with unique graphene-like properties. Transition metal dichalcogenides (TMDCs example MoS_2, WS_2), graphitic carbon nitride (g-C_3N_4), layered metal oxides, hexagonal boron nitride (h-BN) and black phosphorus (BP) are examples of typical graphene-like 2D nanomaterials that manifest versatile properties due to their similar structural features but diverse compositions from graphene [9,10]. In comparison to the conventional organic lubricant additives such as zinc dialkyl dithiophosphate (ZDDP), zinc dialkyl dithiophosphate (ZnDTP) and molybdenum dithiocarbamate (MoDTC), 2D nanosheets show better performance in friction reduction and anti-wear properties and they exhibit enhanced chemical stability which leads to less harmful emissions and lower toxicity, endearing them as a better candidate in terms of environmental sustainability [11–15]. Moreover, their cost of preparation in the area of lubricants is comparably cheap [16]. In this paper, the most recent developments made in the application of some 2D nanomaterials for reduction of friction and wear are reviewed. The aim is to provide a wide-range overview of the recent works on some selected 2D nanomaterials and gain an up to date understanding of their tribological performance.

2. Characteristics of 2D Materials

Materials can be rightly characterized as 2D material or nanosheet if only one of its dimensions is in nano-size, they usually resemble a large sheet with one or few atomic thickness layers (more like a sheet of paper). Since their discovery, they have undoubtedly attracted great academic and industrial interests due to their magnificent array of electronic, optical, physical and chemical properties, which are absent in their bulk counterparts [17]. These unique features are a result of the effect of their spatial confinement in one dimension [18]. Besides, since nanosheets are atomically thin and possess strong in-plane bonds, they are liable to exhibit a remarkable combination of thermal, high mechanical strength and flexibility which are desirable properties for use in various devices [19], which can also result to unusual frictional features [20,21]. The high degree of flexibility associated with 2D materials whenever they are in contact with nearby objects plays a vital role in deciding the real contact area and the frictional pinning potential [22,23]. Besides, the dispersion of 2D materials in aqueous solution are suitable precursors for the design of 2D based films [24], and since all atoms of 2D materials are surface atoms, this provides a proper handle to change the properties of the materials through surface functionalization and modification [25,26].

Notably, layered materials such as graphene, MoS_2, WS_2 and hexagonal BN (h-BN) have long been employed as solid lubricants in numerous engineering applications. The outstanding lubrication performance of these bulk materials is known to be due to the weak interlayer interaction and easy sliding between surrounding atomic layers [27,28]. Recent nanoscale experiments have revealed that layered materials, down to one atomic layer, also show outstandingly low surface friction when they are slid against other counter surfaces [22,28]. Besides weak interlayer interaction, regular atomic arrangements are also known to impact these materials with the potential to achieve super-low friction,

otherwise known as superlubricity [29,30]. Moreover, regarding few-layered 2D materials, it has been shown that the static frictional force gradually increases for a few initial atomic periods before reaching a steady value. Such fleeting behavior and the associated improvement of the steady-state of friction, decreases as the number of 2D layer increases and was observed only when the 2D material was loosely attached to a substrate [23,31]. By employing atomistic simulations, Li et al. reproduce the experimental findings on layer-dependent friction and transient frictional strengthening on graphene nanosheets [23]. Atomic force analysis proved that the evolution of static friction is a demonstration of the innate tendency for thinner and less-constrained graphene to re-arrange its configuration as a direct effect of its higher flexibility. The tip atoms become more firmly pinned and reveal higher synchrony in their stick-slip character. While the quantity of atomic-scale contacts which is the real contact area expands, the local pinning state of individual atoms and the comprehensive commensurability also grows in frictional sliding on graphene nanosheets. Lee et al. [31] analyzed the nanotribological properties of some selected 2D materials such as graphene, MoS_2, h-BN and niobium diselenide ($NbSe_2$) which were separated from their bulk sources using mechanical exfoliation method. It was shown that friction on all the four 2D materials is greater than that of their bulk sources. Their study indicates that the higher friction is associated with the low bending stiffness of the thinnest layers known as the puckering effect. They employed a simple model of a tip sliding across an elastic membrane to understand the mechanism of the sheet stiffness in friction. Herein, when the tip comes in contact with the top surface, there is usually a local puckering because of adhesion [32], this is due to the low bending stiffness of the sheet in relation to its in-plane stiffness. The puckered geometry will be adjusted at the front edge by tip-sheet friction. This out-of-plane puckering might explain the increased friction due to the resultant increase in the tip-sheet contact area. Moreover, it can be due to the extra work required to shift the puckered region. As the sheet becomes thinner, the puckering effect becomes more significant. Besides, graphene, MoS_2 and h-BN possess much lower friction (~1 nN) than $NbSe_2$ (~7 nN). Zhou et al. [33] also demonstrated that TMDCs (MoS_2, WS_2, $MoSe_2$, WSe_2) having smaller vertical interlayer force constant, which is lower elastic modulus, shows more considerable friction when colliding against AFM tips. Furthermore, it is generally known that the kinetic energy during frictional sliding is released electronically or phononically [34,35]. Hence, contrary to what is obtained in bulk lubricants, the unique electrical (or electron-phonon coupling) of 2D materials is considered to have an impact on their frictional behavior [22].

In Summary, the frictional action mechanisms of 2D materials can be described as follows; firstly, because of the very tiny nature of nanosheets, it can penetrate the interspaces of the rubbing surfaces. Under normal force, the relative motion of the rubbing surfaces will provide the needed shear stress leading to the sliding of the interlayers of the nanosheets, thereby reduction of friction and wear. Secondly, there will be a formation of tribofilm at the contact area of sliding surfaces [36,37]. Initially, the formed tribofilm serves as a protective film separating the two rubbing surfaces from direct contact. However, as sliding continues and more heat is generated, a tribochemical reaction is triggered at the contact surfaces between the lubricants and the substrate, this will lead to the rupturing of the protective film and reformation of a new film [4]. This new film is known to significantly enhance tribological behavior [38]. Besides, the high temperature developed during sliding could melt the nanosheets enabling them to fill up the micro-holes, gaps and the concave areas in the contact surfaces, thereby reducing friction and wear [39].

3. Synthesis of 2D Materials

3.1. Mechanical Exfoliation

Over the years, several techniques including mechanical exfoliation, liquid-phase exfoliation, shear exfoliation, epitaxial growth of SiC, unzipping carbon nanotubes and chemical vapor deposition (CVD) have been explored for the synthesis of 2D materials. In 2004, micromechanical cleavage, also known as mechanical exfoliation, was first introduced as an efficient way to produce atomically thin

graphene [7]. Using this technique, single-layer graphene was successfully cleaved from small crystals of highly oriented pyrolytic graphite (HOPG) with the aid of scotch tape, as shown in Figure 1a. The mechanics involve exerting a normal force on a scotch tape, which is applied to the HOPG surface. By continuously repeating this normal force, the graphitic layer gradually thins out until it becomes single-layer graphene from their parent layered bulk crystals [40,41]. This method has also been widely employed in the synthesis of other 2D materials, including TMDCs, h-BN and $NbSe_2$ [42–45]. The outstanding crystal quality with minimal defects make the mechanically cleaved ultrathin 2D materials desired candidates for fundamental study of their inherent physical, optical and electronic properties, and their use in high-performance electronic and/or optoelectronic devices such as transistors and phototransistors. Even though this method is simple and practicable, it is faced with the challenge of non-scalability because of meager output yield and slow output rate. Besides, the process is manually controlled; hence, precision and reproducibility in terms of shape, size and thickness is an enormous challenge [40]. Several researchers have modified the micromechanical cleavage, Shmavonyan and co-workers successfully synthesized monolayer graphene with a larger surface area by additionally separating few-layer graphene near the monolayer region as shown in Figure 1b,c [46]. Moreover, other modifications have been proposed, as described by Peng et al. [47] and Zhang et al. [48].

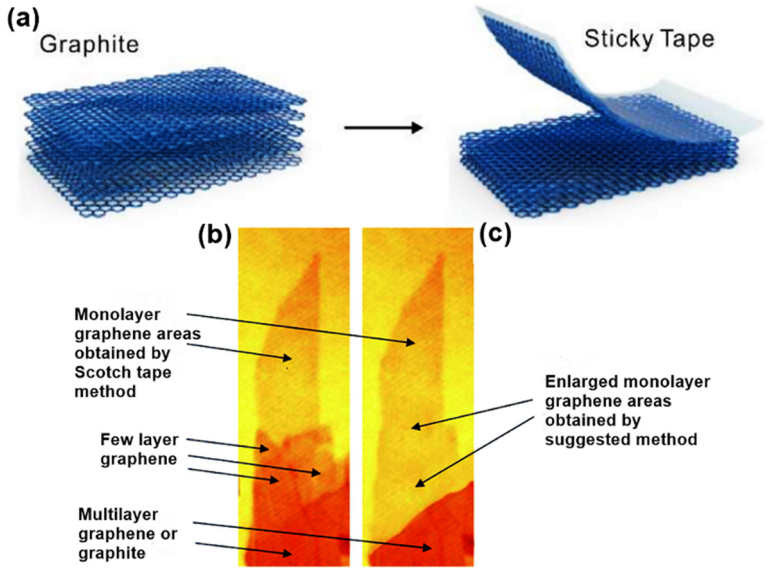

Figure 1. (**a**) Schematic illustration of the mechanical exfoliation of monolayer grapheme [49]. Optical images of monolayer graphene (**b**) as-prepared by scotch tape method and (**c**) as enlarged using Shmavonyan suggested method. Reproduced with permission from [46]. Copyright 2013 National Academy of Sciences of Armenia.

3.2. Liquid-Phase Exfoliation (LPE)

In 2008, Coleman and co-workers used the Liquid-Phase Exfoliation (LPE) technique to synthesize 2D materials [50]. LPE technique involves three steps; first is the dispersion of the bulk materials in a solvent via ultrasonication, secondly is the exfoliation process and thirdly the purification step. The purification step removes the exfoliated flakes from the unexfoliated flakes. To achieve efficient exfoliation using the LPE method, solvents with matching surface energy to the layered bulk crystals are needed; therefore, it becomes challenging getting suitable solvent for each system for each layered bulk crystal. Coleman et al. suggested that the preferred solvents are those that reduced the energy of exfoliation like N-methyl-pyrrolidone (NMP) and isopropanol (IPA) [51]. The Sonication-assisted LPE method is one of the most widely used methods to produce solution-dispersed 2D materials. By controlling the time of sonication, solvent, temperature, power of ultrasonic, surfactants and other additives, one can roughly tune the thickness, concentration and lateral size of the obtained 2D materials. Notwithstanding, there are significant disadvantages of this technique; the production of

single-layer nanosheets is low, the size of the nanosheets is relatively small and for the sonication in aqueous polymer and/or surfactant solution, the available surfactants remaining on the exfoliated nanosheets are not suitable for their applications in optoelectronics and energy storage systems. Besides, the sonication process may impact defects on the nanosheets, which will eventually affect their properties [40].

3.3. Chemical Vapor Deposition (CVD)

Generally, the chemical vapor deposition (CVD) method is believed to be the most promising method for large-scale synthesis of high-quality mono- or few-layer 2D materials. In the CVD process for graphene synthesis, carbonaceous gaseous species react in the presence of metal thin films or foils at high temperatures (900–1100 °C) resulting in the decomposition of the carbon species and the formation of the graphene lattice as illustrated in Figure 2. The growth of the graphene on a metal catalyst is determined by several factors, which include the precursor, carbon solubility limit of the metal, lattice parameters, crystal structure, pressure and temperature of the system [5,52]. By adjusting these conditions, the controlled growth of the graphene with a tunable number of layers, crystallinity and lateral size can be obtained [53]. Somani et al. reported the synthesis of planer few-layer graphene (PFLG) by thermal CVD method [54]. They grew the PFLG using low-cost camphor on a nickel substrate. In 2009, Xuesong and co-workers used the CVD technique at 1000 °C to grow large-area high-quality single-layer graphene films using a mixture of methane and hydrogen gas as the carbon precursor on a copper foil substrate [55]. Methane, acetylene and ethylene are the common gaseous carbon precursors used in synthesizing graphene. Among them, methane is known to be the most effective carbon source for graphene synthesis.

Ethylene has also been widely employed besides methane because the relatively high reactivity of ethylene decreases the temperature required for graphene growth using the CVD process. Researchers have also tried several other metals besides Ni, such as Cu, Ir, Ru, Co, Pt, Pd and Re, which have different carbon solubility and catalytic effects. High-quality single-layer graphene grown on polycrystalline Cu films has drawn a lot of interest because it has an advantage of proper control of graphene layers, transferability and low cost [53]. The CVD method has also been employed in the production of large-scale 2D TMDC nanosheets, including alloyed 2D TMDC [40]. Zhan et al. were among the first to show the growth of MoS_2 on Si/SiO_2 substrate [56]. This was achieved by the deposition of Mo thin film on the Si/SiO_2 substrate, followed by the CVD process. The Mo-coated substrate and sulfur powder were kept in a CVD furnace in an inert environment under a constant flow of Nitrogen gas. The temperature was increased to 750 °C and stayed for 90 min, giving time for Mo to react with evaporated sulfur, resulting in the growth of single/few layers MoS_2 on Si/SiO_2 substrate [40,56].

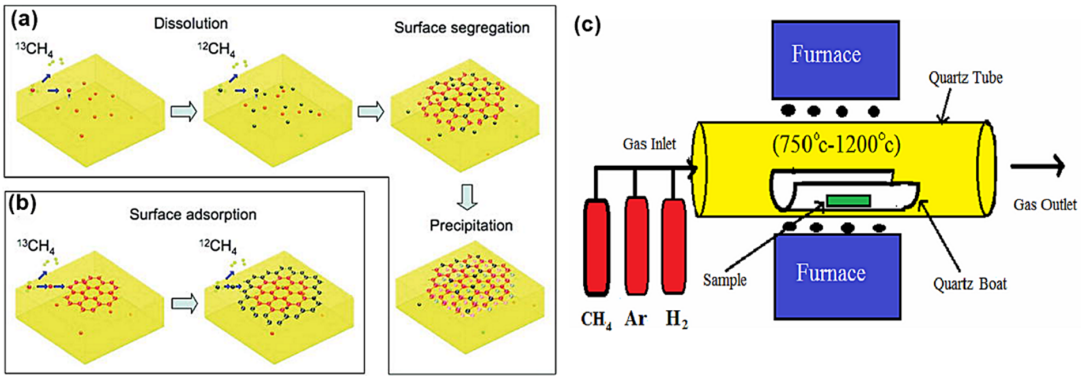

Figure 2. (**a**,**b**) Schematic demonstration of the growth mechanism of graphene. Reproduced with permission from [57]. Copyright 2009 American Chemical Society. (**c**) Schematic illustration of the CVD process setup. Reproduced with permission from [58]. Copyright 2015 CSIR-NISCAIR.

4. Tribology of 2D Materials

4.1. Graphene and Graphene-Family

Graphene is known to possess high degrees of stiffness, strength, thermal conductivity and impermeability to liquid and gas. Besides, the combination of outstanding physical and chemical properties together with low cost of production makes graphene a better candidate of choice in nano-electromechanical and miniaturized devices [5,59]. The atomic thickness of graphene notwithstanding, it is one of the known most durable materials with intrinsic strength of 130 GPa and fracture toughness of 4.0 ± 0.6 MPa$\sqrt{m}$ and Young's Modulus of 1 TPa [22,60]. The superior strength and high thermal stability (above 3000 W/m·K) of graphene offers great potential for use as ultra-thin protective coatings for several precision components exposed to contact stress [5] and also serve as an ideal candidate for a host of MEMS and NEMS where atomically thin solid lubricants and outstanding anti-wear performance is desired [22]. Besides, these excellent properties of graphene enable it to sustain a more permanent and highly-efficient lubricating performance even under severe tribological conditions such as extreme pressure, extreme temperature and extreme mechanical stresses [61]. Because graphene exhibit impermeability to liquids and gases such as water or oxygen, it will slow down the oxidative and corrosive activities that are destructive to the rubbing surfaces [62]. At room temperature, graphene has high electron mobility (2.5×10^5 $cm^2 \cdot V^{-1} \cdot s^{-1}$) along the in-plane direction [36] in suspended conditions. As shown by angle-resolved photoemission spectroscopy and scanning tunneling spectroscopy, the electron-phonon interaction strength of graphene is dependent on sample thickness and local interactions with substrates [36].

At the initial period of sliding a tribopair, a change in the interfacial property (such as friction force, wear rate and surface deformation) usually occurs. This transient, non-steady-state change is generally known as "running-in" [63,64]. Running-in is commonly known to be a result of the change in the interfacial roughness and the wear of contact asperities [65]. However, in practice, changes in the microstructure, surface composition and third body might also result in running-in. Recently, Zhao et al. observed a running-in phenomenon occurring in single-layer graphene grown on a Cu substrate [66]. They scratched the graphene surface repeatedly with the tip of an atomic force microscope (AFM), it was observed that the frictional force decreases by 32.6% at ~62 scratching cycles before approaching a steady-state (stable till 256 cycles). In contrast, the graphene coating is free of wear and damage. To understand the mechanism behind this interesting observation, the normal load and sliding velocity were changed and a nanoindentation test was performed. It was shown that the running-in process was as a result of the plastic deformation and hardening of the underlying Cu substrate. Yao et al. [67] used AFM nano-scale scratch experiments on graphene transferred on four different substrates such as PDMS, epoxy, SiO_2 and sapphire to show that the antiwear performance of graphene, which is usually characterized by the maximum load-carrying capacity, is not a function of the intrinsic material property. Instead, its value is mostly affected by the substrate's stiffness, as represented in Figure 3. Typically, a stiffer substrate yields a higher load-carrying capacity. The Finite Element Analysis (FEA) simulations showed that a more rigid substrate can effectively distribute the normal load and reduce the in-plane stress of graphene by inhibiting graphene deformation, which improves the overall load carrying capacity. Besides the load sharing mechanism, their experimental results also showed that the frictional shear stress during scratch tests may promote wear of graphene by reducing its equivalent strength.

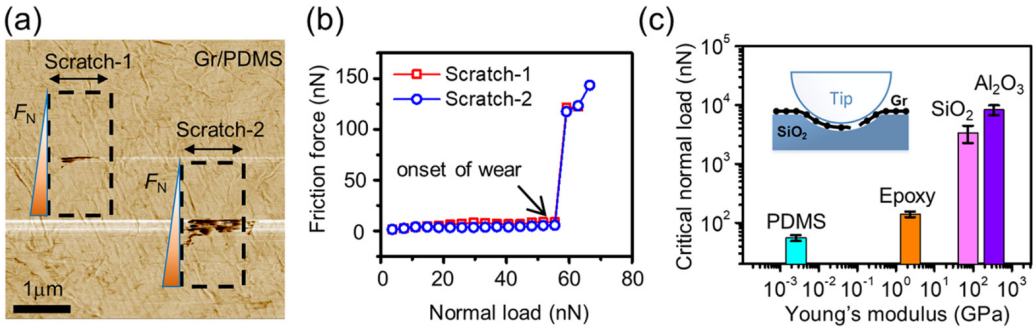

Figure 3. (**a**) A lateral force image of graphene/PDMS sample done under a low load after two scratch tests; the black arrows indicate the scratch direction. (**b**) Variations of friction with the normal load during the scratch tests in (**a**). (**c**) Critical normal loads of graphene on the substrates with different stiffnesses. Reproduced with permission from [67]. Copyright 2019 AIP Publishing.

4.1.1. Influence of Solvent

It has been proven that some low molecular weight vapors such as water under ambient conditions are needed for graphite to work as a solid lubricant. Several experimental results have shown that the vapors cast physisorbed molecular layers on the surface of the graphite and there is a noticeable increase in friction when the physisorbed layers evaporate [68,69]. Besides, fast water penetration via graphene capillaries within graphene oxide membranes has shown that there is low friction of water flow along graphene surfaces, suggesting that the sliding of graphene is lubricated by water. This result has also been supported by Computer simulations [70–72]. Lin et al. investigated the effect of interface hydration on the sliding of 2D materials (Figure 4). They proved that when the interfaces between a mica substrate and single-layers of graphene and MoS_2 is hydrated with a molecularly thin layer of water, it usually affects the transfer of strain from the substrate to the 2D materials. The strain in graphene and MoS_2 were detected by the changes in Raman and photoluminescence (PL) spectra, respectively. It was observed that the strain relaxation in graphene changes from stick-slip in dry contact, to viscous when hydrated. However, viscous relaxation was not seen in MoS_2, despite hydration [73]. Moreover, the relaxation of graphene at the hydrated interface is slower when compared with the dry interface. This is probably due to the increase in the density of flexural phonons in graphene, which results in higher friction [74]. Lee and co-workers had already provided a clear picture of the elementary mechanisms for the dissipation of energy in friction and the role of intercalated molecular water films. They used graphene flakes deposited on mica substrate with intercalated water to demonstrate that the excitation of the vibration of atoms at the contact interfaces, where there is an increase in the availability of vibration modes improves friction. The transfer of energy from surface vibration to the bulk of the substrate are the two critical mechanisms responsible for energy dissipation in friction. They reported that the friction increased by a factor of ~3 in relation to the dry mica substrate. Besides, density functional theory (DFT) calculations revealed that water expanded the spectral range of graphene vibrations, especially the low-frequency flexural modes, thereby providing new excitation routes and also by widening the overlap with the atomic vibrations of the mica substrate, which promotes coupling and energy transfer [74]. Several other studies have shown that water can easily intercalate between graphene and hydrophilic substrates such as mica and silicon oxide [75–78].

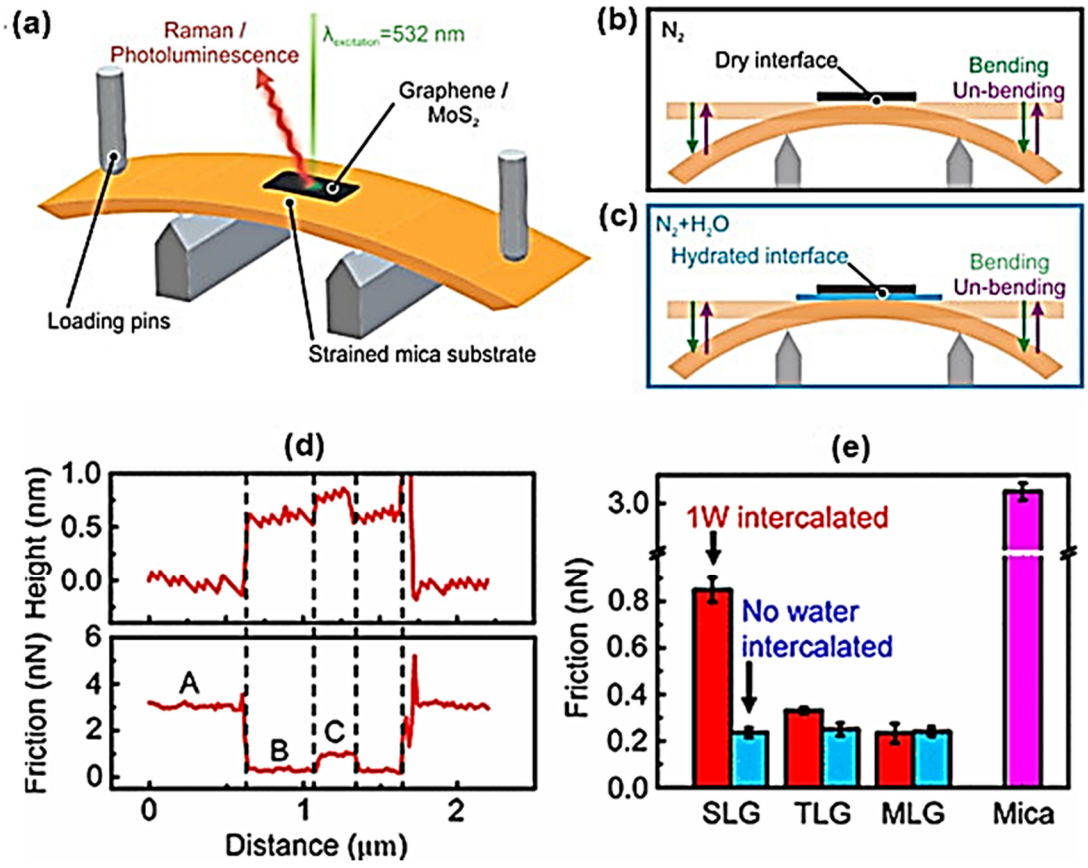

Figure 4. Hydration and strain transfer test between the interfaces of mica substrate and 2D materials: (**a**) Illustration of the four-point bending setup. Strains in graphene and MoS_2 flakes were, respectively, detected with Raman and photoluminescence (PL) peak positions, for both (**b**) dry and (**c**) hydrated interfaces. Reproduced with permission from [73]. Copyright 2019 Elsevier. (**d**) Line graph of the height (top) and friction (bottom) obtained by subtracting the retrace from the trace signals along the solid red lines A–C. (**e**) Comparison of the friction force on the graphene regions with various numbers of stacked graphene layers, with and without intercalated water. SLG, TLG and MLG represent single-, tri- and multilayer graphene on the mica substrate, respectively. The red bars show a monolayer (1W) of intercalated water. The blue bars indicate friction without intercalated water. The purple bar on the right indicates bare mica. Reproduced with permission from [74]. Copyright 2017 American Chemical Society.

4.1.2. Applications as Lubricant Nano-Additives

Recently, the application of nanomaterials as superior solid lubricants or nano-additives has drawn massive interest due to their unique attributes like a smaller size, chemical and thermal stability [36,79]. These nanomaterials can easily form a shearing thin film at the sliding contact interface giving rise to low friction, also can fill and/or repair the micro/nano cracks formed on the worn surfaces, showing comprehensive advantages for enhancing the tribological performances of lubricant oils [61]. Mutyala and co-workers [80] employed a composite mixture of graphene and MoS_2 as a solid lubricant to decrease friction and wear in steel hydrogenated diamond-like-carbon (H-DLC) contacts operating at high contact pressures and sliding speed. The sliding friction tests carried out under dry nitrogen conditions revealed a reduction of friction by 16 times and wear by 29 times, as compared to Steel vs H-DLC (baseline) experiments, as shown in Figure 5. Moreover, a reduction of friction by a factor of 43 and wear by a factor 434, as compared to self-mated steel against steel experiments. The TEM images confirmed the deposition of tribolayer on the ball and disc and the wear debris is made up of amorphous carbon mixed with graphene layers. Primary mechanism is ascribed to the tribochemistry

resulting in the formation of amorphous carbon by active disintegration of MoS_2 at the tribological interface under the influence of high contact pressure. Besides, they conducted further experiments with pure graphene and pure MoS_2 under the same test conditions. The results revealed a friction coefficient of 0.114 for pure graphene and 0.218 for pure MoS_2. Notably, both the friction and ball wear rate for Steel-DLC contacts with pure graphene and pure MoS_2 were greater than combined Graphene and MoS_2 solid lubricant [80,81].

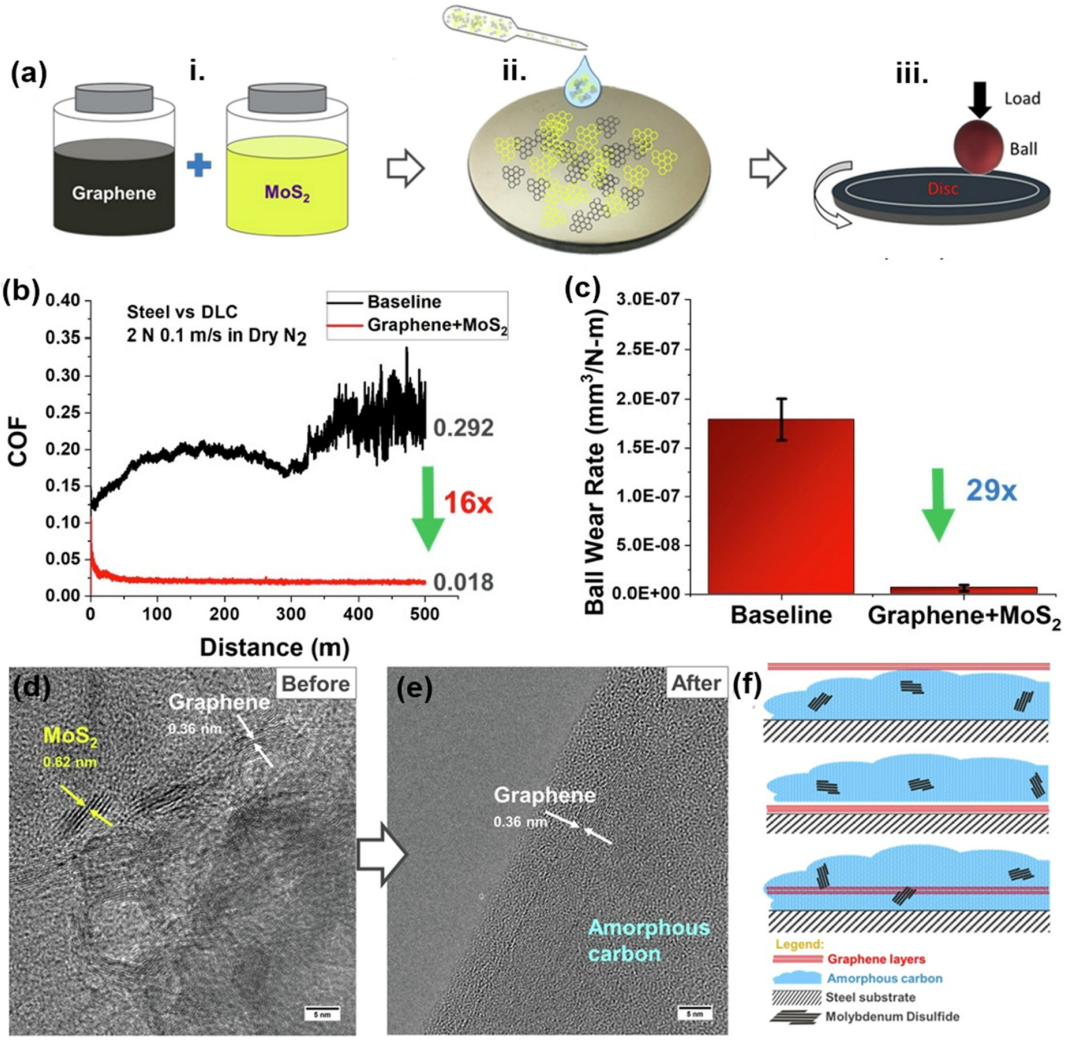

Figure 5. (**a**) Graphene + MoS_2 solid lubricant via drop-casting method: (i) Mixing of the solution-processed graphene and MoS_2, (ii) Drop-casted onto steel disc and (iii) Ballon-disc configuration test. (**b**) COF graph for Baseline and Graphene + MoS_2 tests, (**c**) Comparison of ball wear rate for the Baseline and Grapehene + MoS_2. TEM pictures indicating the (**d**) presence of Graphene and MoS_2 in the as-prepared solid lubricant prior to testing and (**e**) the wear debris is made up of graphene layers mixed in amorphous carbon. (**f**) Mechanistic model describing graphene mixed amorphous carbon in different configurations with partly disintegrated MoS_2 layers. Reproduced with permission from [80]. Copyright 2019 Elsevier.

Wei et al. [82] used 2D lubricant additives such as graphene oxide (GO), functionalized graphene (GF) and a mixture of WS_2/Graphene processed in an alcohol solution to improve the tribological properties of ultrafine-grained graphite HPG510. They deposited the different 2D lubricant additives processed in alcohol on the HPG510 substrate. Their findings showed that the coefficient of friction of the graphite was decreased from 0.25 to 0.06 when lubricated by the 2D materials processed in an alcohol solution. Besides, the addition of the 2D lubricants decreased the wear of the balls and graphite

substrate and the amorphization of graphite was suppressed as shown in Figure 6. The mechanism is that 2D lubricants did not just offer a lubricating effect to reduce COF of graphite because of the inherent low shear strength of the layered structure, the 2D lubricants also enhanced the loadbearing ability of the graphite substrate, resulting to improved wear resistance. This is because of the higher load-bearing capacity of 2D materials.

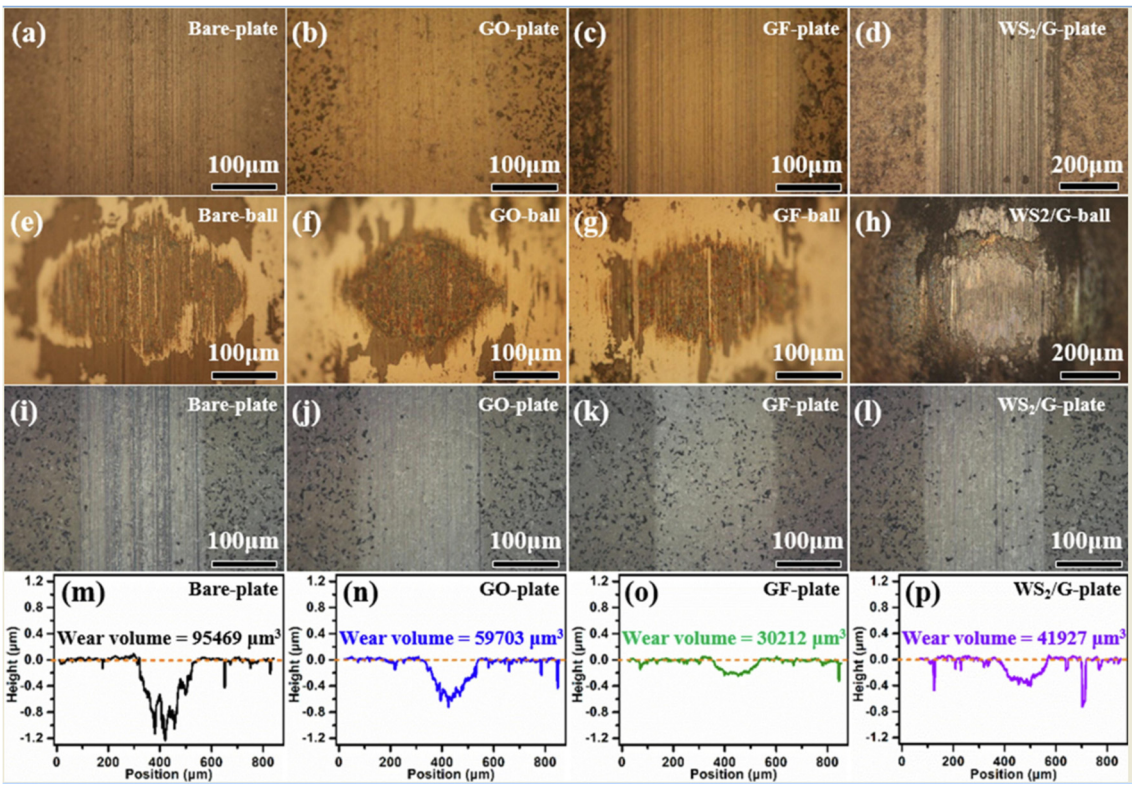

Figure 6. The optical images showing: (**a**–**d**) The surface wear morphologies of the graphite plates and (**e**–**h**) the corresponding counter facing bearing steel balls after lubrication by the 2D lubricant additives for 12,000 cycles of frictional test, (**i**–**l**) the surface wear morphologies of the graphite after lubrication by the 2D lubricant additives before the complete evaporation of the alcohol, (**m**–**p**) the corresponding wear depths and wear volumes of the graphite. Reproduced with permission from [82]. Copyright 2020 Elsevier.

Zhu et al. employed a novel small-size and alkyl-functionalized reduced graphene oxide (RGO-g-OA) exhibiting high dispersion capacity to improve the tribological performance of a lube oil [61]. The novel RGO-g-OA was synthesized using three key steps, as depicted in Figure 7; mechanical crushing of GO to give smaller-sized GO, then surface grafting through an esterification reaction using octadecyl alcohol (OA), followed by incomplete chemical reduction with L-ascorbic acid as illustrated. Specific amounts of the novel RGO-g-OA were dispersed in a finished oil and the tribological performance was evaluated.

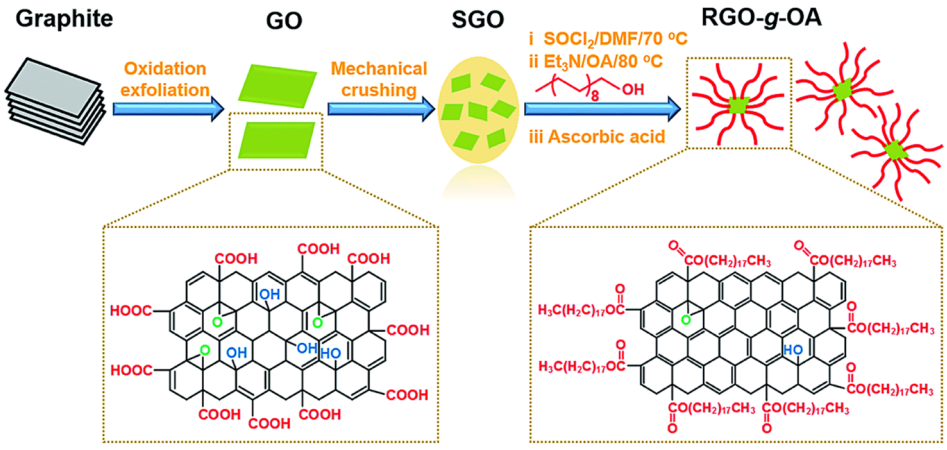

Figure 7. Schematic of preparation procedures for RGO-g-OA. Reproduced with permission from [61]. Copyright 2019 Royal Society of Chemistry.

The finished oil modified with RGO-g-OA nano-additives at a very low content (0.005 wt.%) gave an outstanding friction reduction and anti-wear performances. The corresponding friction coefficient and wear volume were significantly reduced to 0.065 and 10316 μm^3, by 9.7% and 44%, respectively, in relation to those of original finished oil (Figure 8). The ultrafine RGO-g-OA is believed to have formed continuous protective tribofilm between rubbing surfaces preventing them from having direct contact, resulting in the reduction of friction and wear. Han et al. utilized alkyl functionalized graphene oxide (FGO), inorganic fullerene-type WS_2 (IF-WS_2) and 1-methyl-2,4-bis (Noctadecylurea) benzene (MOB) which is a gelator to improve the tribological performance of polyalphaolefin4 (PAO4) lubricant oil. The friction test proved that the combined mixture of 0.1 wt.% FGO6, 1.0 wt.% IF-WS_2 and 1.0 wt.% MOB decreased the COF and size of wear scar by 13.06% and 21.18%, respectively, compared to PAO4 oil with solid lubricants [83].

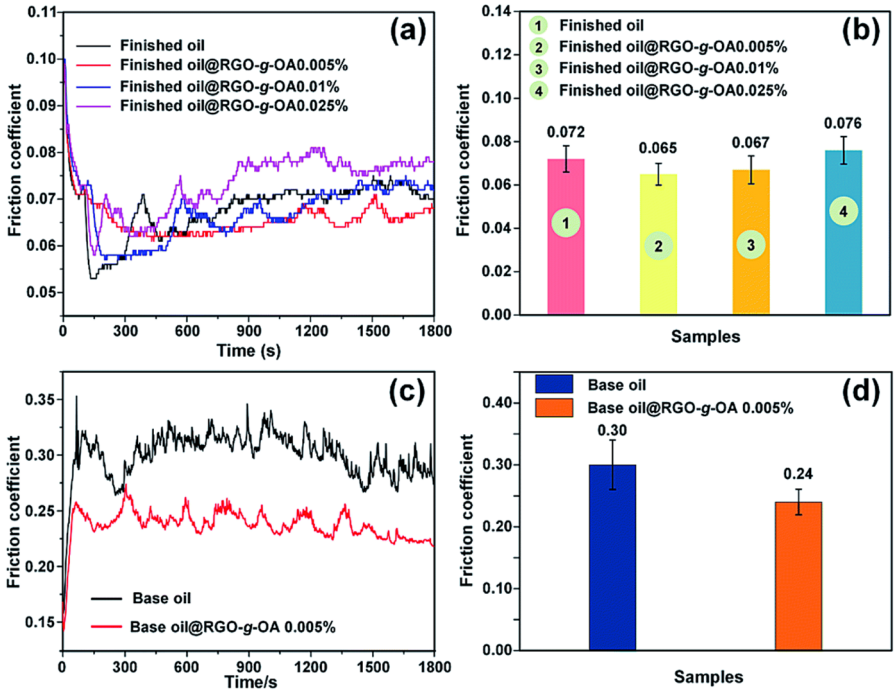

Figure 8. (**a**,**c**) Typical friction coefficients with time and (**b**,**d**) average friction coefficients of pristine finished oil, base oil and the ones filled with various mass contents of RGO-g-OA on steel discs; the load applied is 100 N. Reproduced with permission from [61]. Copyright 2019 Royal Society of Chemistry.

4.1.3. In Combination with Non-2D Materials

Berman et al. [84] illustrated that solid lubricants consist of graphene mixed with iron nanoparticles under high contact pressures at the sliding interface can undergo tribochemical reactions resulting in the formation of onion-like-carbon nanostructures (OLCs) giving rise to superlubricity (~0.0009 COF) in dry N_2 environment (Figure 9). The formation of the OLCs is ascribed to the common tribochemical reaction, which was initiated by Fe nanoparticles with neighboring graphene and carbon debris formed in the sliding process. Graphene is known to self-assemble or aggregate [85]. Hence, as surrounding graphene envelops the Fe nanoparticles, high contact pressure and shear followed by the local rise in temperature causes the graphitization of carbon and converts them into OLCs, resulting in superlubricity. They employed molecular dynamic simulation to further demonstrate the mechanism of the formation of OLCs. Moreover, they proved that the introduction of Fe oxide nanoparticles into the sliding interface can trigger the antagonistic effect of the oxide shell which prevents OLCs formation and in turn suppressed superlubricity.

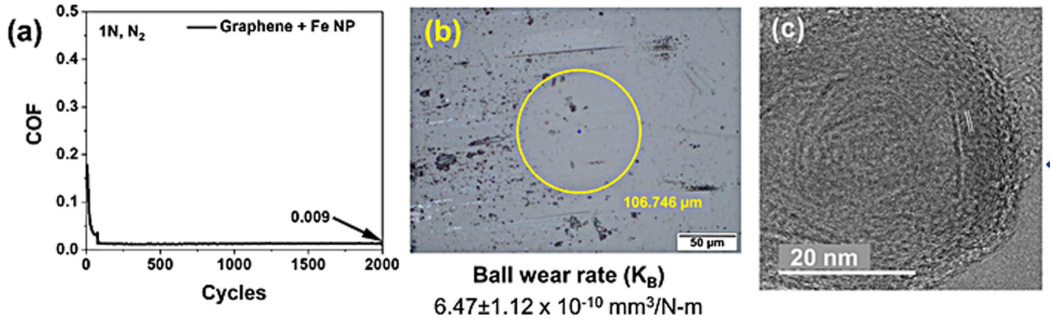

Figure 9. Iron nanoparticles mixed with graphene flakes and sliding against the hydrogenated diamond-like-carbon surface: (**a**) COF (0.0087 ± 0.0008) and (**b**) DLC ball wear diameter and estimated ball wear rate. (**c**) TEM image of wear debris collected from the wear track after 500 wear cycles, revealing a well-formed onion-like carbon nanostructure. Reproduced with permission from [84]. Copyright 2019 John Wiley and Sons.

Ge and co-workers [86] applied the synergistic effect of graphene oxide (GO) and ionic liquid to achieve a robust macroscale liquid-superlubricity state (~0.005) under very high pressure of 600MPa between the frictional pairs of Si_3N_4/sapphire. They suggested that a composite boundary layer produced by the ionic liquid at the interface added to the excellent antiwear ability, hence supplying a lubricating condition under very high pressure. Moreover, GO nanosheets were seen to adsorb on worn surfaces indicating the transformation of the shear interface from Si_3N_4/sapphire into GO/GO nanosheets. The very high-pressure property and extremely low shear stress between the interlayers of GO nanosheets are believed to contribute to the attainment of superlubricity.

Srivyas et al. [87] studied the tribological performance of graphene nanoplatelets (GNP) as a secondary reinforcement in a hybrid aluminum composite. Varying amount of GNP was added to the Al-Si-6 wt.% Al_2O_3 composite. PAO base oil and SAE20W50 Engine oil lubricants were used. The tests revealed the coefficient of friction remained stable as the sliding distance increased. The COF decreased as the normal load increased before attaining a steady stable state. The reason behind the low friction and wear is the outstanding lubricating influence of the GNP layer as it mixes with the lubricating oil. The GNP particle layer is believed to form a low shear stress junction protective layer at the sliding interface, which causes easy shear due to weak Vander wall force, hence, reduction of friction and wear of the hybrid composite.

4.1.4. Biomedical Application

In a bid to extend the tribological performance of 2D materials in biomaterial application especially in scaffolding, Taromsani et al. [88] reported on the effects of graphene nanoplatelets (GNP) and

hydroxyapatite (HAp) nanopowder on the microstructural, tensile, wear and biofunctional properties of medical grade ultra-high molecular weight polyethylene UHMWPE based nanocomposites, to explore GNP's wear resistance and mechanical strength. Varying percentages of GNP with 10 wt.% optimized concentration of HAp were added to the UHMWPE matrix. The mechanical analysis showed a 114% increase in elastic modulus and a 24% increase in yield strength for the sample with 1 wt.% GNP and 10 wt.% HAp as compared to UHMWPE only. Besides, 0.5 wt.% GNP containing sample offered highest tensile performance with an increase of 101% and 31% in elastic modulus and yield strength, respectively, indicating that the strengthening mechanism is significantly influenced by the ratio of the reinforcement, particularly in regards to 2D reinforcing phases such as GNP. Besides, the pin-on-disk tribological analysis revealed a kind of similar result for the COF, The COF decreased by 50% for 1 wt.% GNP sample and 54% decrease for 0.5 wt.% GNP sample. Moreover, a general trend of decrease was observed as regards wear rate where 82% decrease was seen in the 1 wt.% GNP sample. Several other pieces of research have gone on to confirm the potential of graphene in biomaterial applications and their biocompatibility [89–91].

4.2. Transition Metal Dichalcogenides (TMDCs)

TMDCs are a structurally and chemically well-defined family known with a chemical formula of MX_2, where M represents the transition metal element and X indicates a chalcogen (S, Se or Te). The 2D arrangement of MX_2 materials impacts them low shear resistance to each applied shear stress and reduces friction at the interfaces [4]. Ultra-thin 2D TMDCs are technologically captivating and, contrary to the graphene nanosheet, they are chemically all-purpose. The tunable electronic structure has made TMDCs very attractive for numerous applications.

4.2.1. Molybdenum Disulfide (MoS_2)

MoS_2 is a typical representative TMDC which has gained a great deal of research interest. The superior mechanical flexibility (Young Modulus of 0.33 ± 0.07 TPa) and low frictional characteristics of 2D MoS_2 shows that it can serve as an effective protective or lubricant layer for NEMS and MEMS which encounters contact sliding during operations [92,93]. Recently, Serpini et al. [94] employed AFM in the lateral force mode (LFM) as an experimental sliding device to study the tribological behavior of MoS_2 at the nanoscale. Two different samples MoS_2 (disordered sputtered MoS_2 and molybdenite single crystal) were considered and they sputtered the AFM tips with MoS_2 film of varying thicknesses. The deployment of the MoS_2-sputtered atomic force microscopy tips enabled the study of the frictional properties of MoS_2 against itself, therefore, characterizing the sliding dynamics happening within the MoS_2 layers. The reported average values of COF for the sputtered-deposited MoS_2 coating in nitrogen and high humidity (RH 95%) atmosphere are 0.41 ± 0.05 and 0.58 ± 0.06, respectively. Whereas for the single-crystal MoS_2, the average COF value in nitrogen is 0.0121 ± 0.0017 and in high humidity is 0.013 ± 0.005. The results indicate that the influence of humidity on the friction behavior of a single crystal MoS_2 is very minimal. This can be ascribed to the fact that for an almost perfect crystalline structure, only very few of the edges are naked to water molecules. Similar observations have been reported elsewhere [95,96]. Besides, the notable difference between the COF in dry nitrogen of the single crystal and the disordered-sputtered coating was explained as follows. When the contact is between two ordered layers, the sliding process is shown as continuously overcoming the weak van der Waals forces between MoS_2 layers. However, this explanation is believed to hold for nanoscale, because at micro/macro-scale other purely dissipative activities are also considered. However, when the contact is between two amorphous layers, the sliding process includes the overcoming of van der Waals forces and the breaking of covalent bonds which forms between the two surfaces as a result of unsaturated bonds. They also employed Molecular dynamics simulations to corroborate their finding.

Cao et al. evaluated the anisotropic nanofriction force on MoS_2 of varying thicknesses using AFM in ambient air [97]. The periodicity of nanofriction force on MoS_2 of 45.23 nm thickness is shown to be ~180°, the same as the sawtooth-type lattice periodicity of MoS_2. Typically, quasi-2D material such

as MoS_2 shows a sawtooth-like and sandwich structure [98]. The identified anisotropic nanofriction on MoS_2 of 4.18 nm thickness was ascribed to the combined influence of the lattice orientation and puckering effect. The anisotropic nanofriction on MoS_2 of 1.49 nm thickness is duly as a result of the puckering effect. Moreover, an increase in the thickness of MoS_2 results in the decrease of the nanofriction and the increase in the anisotropy ratio of nanofriction. Acikgoz and co-workers [99] studied the influence of sliding speed on the frictional behavior of single-layer and bulk MoS_2 using AFM experiments. They concluded that friction forces increase logarithmically with the increase in sliding speed. Moreover, there is no correlation between the speed-dependence of friction and the MoS_2 layer number and changes in the speed-dependence of friction can be ascribed to the changes in the physical behavior of the AFM probe in the form of the different contact stiffness and tip's interaction potential variables in the thermally activated Prandtl–Tomlinson model.

In order, to improve the dispersibility and stability of MoS_2, Wu et al. [100] used oleic diethanolamide (OD) to modify MoS_2 nanosheets, thereafter study the tribological behavior in base-oil using a four-ball tester. The results showed that the average COF and average wear scar diameter of 0.08 wt.% OD-MoS_2-based oil were reduced by ~36.8% and ~15.4% as compared with the base oil, respectively. Moreover, its extreme pressure performance increased by ~15.2%. Li and co-workers evaluated the influence of oxidizing gases (O_2 and H_2O) on the tribological characteristics of MoS_2 coating in sliding contact against 52100 steel bearing ball and found them to be beneficial [101]. They reported that a small amount of the oxidizing gases can impact structural disorder and defect of MoS_2 at the sliding interface. This will increase the adhesion strength between transfer films and the tribopairs, thereby enhancing the tribological actions of MoS_2 coatings.

Chen et al. [102] investigated the tribological properties of epoxy coating reinforced with a novel hybrid of 2D h-BN/MoS_2 (Figure 10). They observed that the COF and wear rate of the epoxy composite coating decreased by ~80% and ~88% as compared to pure epoxy. The composite coating still kept outstanding tribological properties under high load or sliding conditions. This is due to the excellent dispersibility of MoS_2, high actions of h-BN and synergistic improving effect of h-BN/MoS_2, including the deposition of transfer film on the sliding surface. Recently, Yu et al. [103] achieved a superlubricity state (COF 0.004 ± 0.001) by combining the synergistic effect of hydrogenated diamond-like carbon (H-DLC), MoS_2 and hydrogen-free diamond-like carbon (DLC).

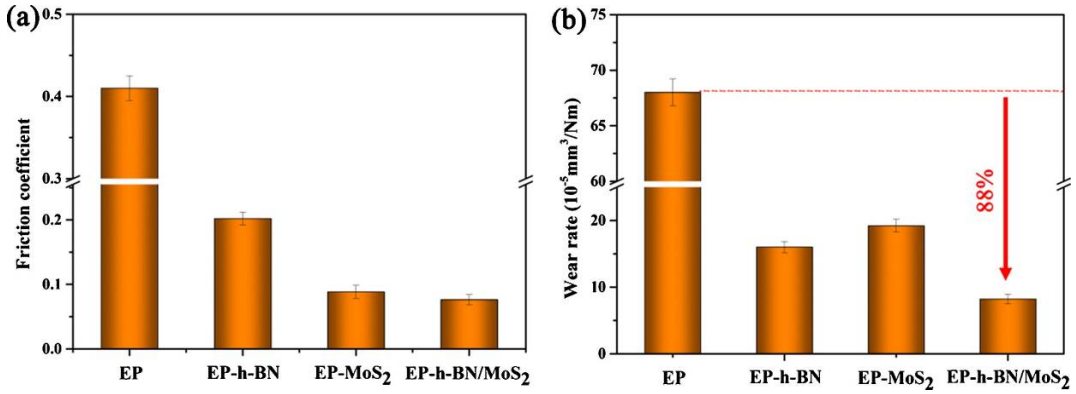

Figure 10. (**a**) Coefficient of friction and (**b**) wear rate of EP, EP-h-BN, EP-MoS_2 and EP-h-BN/MoS_2 composite coatings sliding against 440c ball under dry friction (EP = epoxy). Reproduced with permission from [102]. Copyright 2010 Elsevier.

4.2.2. Tungsten Disulfide (WS_2)

Another member of TMDCs which has attracted a great deal of research interest is WS_2 nanosheets. Specifically, WS_2 nanosheets are known to exhibit excellent tribological performance under high temperatures [104,105]. Moreover, it has been reported to show outstanding tribological properties as a nano-additives in lubricant oil, they can react with the metal substrate to generate layered tribofilms and

can efficiently decrease friction and wear under boundary lubrication condition [15,106,107]. Recently, Ma et al. [108] recommended a novel approach to produce a high-quality WS_2 nanosheet through the microwave-assisted liquid-phase sonication. The resultant WS_2 gave an excellent tribological performance in base-oil. The average COF and wear scar diameter of the WS_2 nanosheets-based oil were decreased by 28.47% and 51.67% as compared to the oil, respectively. Hu and co-workers investigated the tribological behavior of WS_2 with different morphology (lamellar WS_2 and spherical WS_2) under varying loads and speeds conditions [109]. They proved that the COF of lubricating oil with lamellar WS_2 additive was reduced by 29.35% at the optimal condition and the minimum COF was recorded at ~100 N. The COF of lubricating oil with spherical WS_2 additive decreased by 30.24% and the minimum COF was observed at 120 N. The high-pressure behavior of spherical WS_2 was better than that of lamellar WS_2. The spherical WS_2 gave a more stable wear resistance at over 80 N loads. The explanation given for the major difference in the tribological behavior mechanism of the WS_2 with different forms was as follows; for WS_2 with lamellar structure, the lamellar structure improved the slip between layers and the surfaces of layers resulting in the decrease in COF. While, the spherical structured WS_2, its spherical structure is considered as a 'small ball', which can play a role akin to 'micro-bearing' on the friction surface, turning the sliding friction between surfaces into rolling friction thereby decreasing the COF.

Application in Low Earth Orbits (LEO)

In low earth orbits (LEO), the oxidation and erosion of atomic oxygen are known to be the most critical environmental factor for materials used in the aerospace environment. For preserving the service-life of spacecraft and ensuring reliability, more considerable attention is given to the response behavior of spacecraft materials to the atomic oxygen environment. Xu et al. investigated the tribological performance of sputtered WS_2 films possessing loose or dense microstructures in a vacuum, atomic oxygen (AO) and vacuum/AO irradiation alternate conditions [110]. Their finding shows that the WS_2 films revealed a periodic fluctuant COF and high wear under the simultaneous action of atomic oxygen irradiation and friction (in-situ condition). They proved that the friction and wear characteristics are not dependent on the film compactness but the anti-oxidation ability of WS_2 itself. Concerning the in-situ atomic oxygen irradiation condition, the high friction is due to the formation of oxidation product (WO_3) by AO and its delamination by frictional interaction was the cause of the high wear. They suggested that improving the anti-oxidation ability of WS_2 instead of just densify the film microstructure is the best way to effectively enhance the wear resistance of WS_2 film in the potential service environment. Fu et al. [111] investigated the influence of atomic oxygen on MoS_2-WS_2 composite lubricating film. The composite film has a dense film microstructure and shows excellent atomic oxygen resistance due to the doping of WS_2. They reported that the introduction of WS_2 to the MoS_2-based film altered the film structure and enhanced the oxidation resistance of the film. In comparison to pure MoS_2 film, the wear rate of the composite film was decreased by 53% at 20 r/min, 68% at 100 r/min and 30% at 200 r/min as shown in Figure 11. Gao et al. have reported similar results [112].

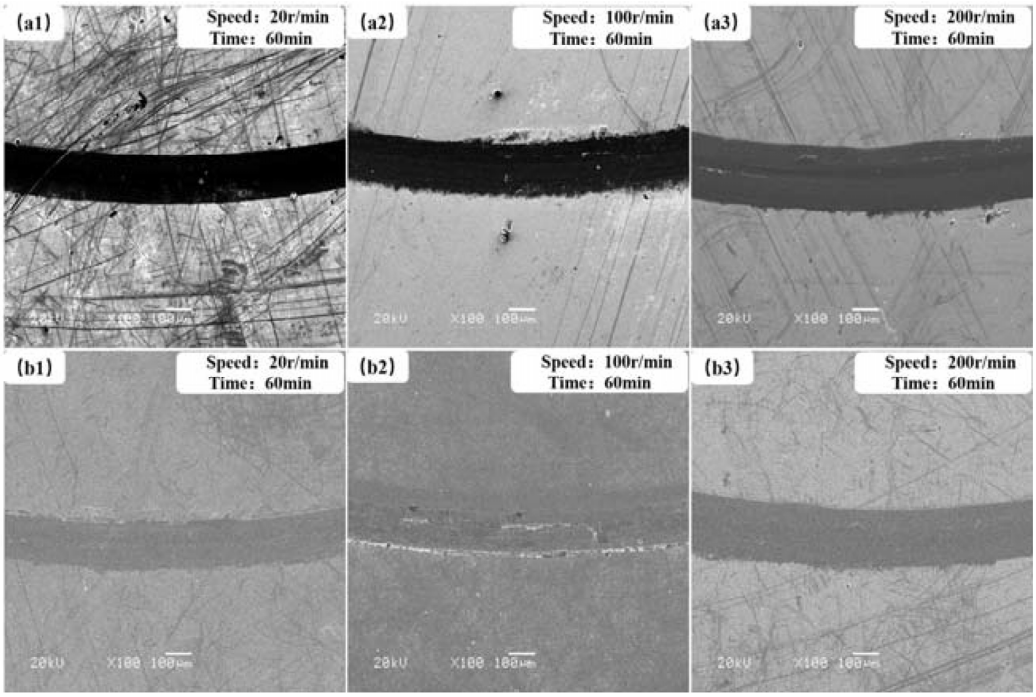

Figure 11. The morphologies of the wear tracks for pure MoS_2 film (**a1**–**a3**) and the MoS_2–WS_2 composite film (**b1**–**b3**) after atomic oxygen irradiation at varying sliding speeds. Reproduced with permission from [111]. Copyright 2020 MDPI AG.

4.3. Other 2D Layered Materials

4.3.1. Zirconium Phosphate

Along with the various 2D nanomaterials employed in lubricating oils, layered-zirconium phosphate ($Zr(HPO_4)_2{\cdot}H_2O$, α-ZrP) nanosheets have also gotten broad research interest for a wide range of lubrication applications due to their unique 2D layered structures, easy surface modifications and high purity. He et al. has shown that α-ZrP nanoplatelets were very effective as lubricant nano-additives in both non-aqueous and aqueous media. The COF was decreased by 65% and 91% in mineral oil and water, respectively [113]. Dai et al. studied the tribological performance of α-ZrP particles as a nano-additive in anhydrous calcium grease. Their results proved that the anti-wear behavior and load-carrying capacity of lithium grease largely improved due to the formation of a stable and compact tribofilm with low shearing strength during the rubbing surfaces. Meanwhile, the poor dispersion of unmodified α-ZrP in oil has limited their tribological performance. Therefore, efforts have been made to improve α-ZrP dispersibility. Jiang et al. synthesized 2D layered α-ZrP nanosheets intercalated with varying amines content and studied their dispersion stabilities in lubricating oil and tribological properties. The results revealed that with the introduction of well-dispersed zirconium phosphate nanosheets, the COF and pin volume loss decreased by ~47% and 75%, respectively. The outstanding dispersion stability made the nanosheets flow into the contact area at the inception and hence protect the contact surface. The mechanism is that the decrease in the van der Waals forces between the adjacent layers impacted by the intercalated amines changed the friction between adjacent layers from pin disk to sliding, resulting in a reduced COF under hydrodynamic lubrication.

4.3.2. Hexagonal Boron Nitride (h-BN)

Hexagonal boron nitride (h-BN) nanosheet is another 2D material that has huge potential as a solid lubricant; it exhibits a good combination of chemical stability, high mechanical strength, thermal conductivity and low density of surface dangling bonds. Besides being desirable as the part of core/shell assemblies, h-BN also shows superior tribological behavior amid other BN nanostructures like spherical,

hollow, rod-like and prismatic nanoparticles [114,115]. They have also attracted particular interest in superlubricity operations. Sagbas et al. improved the tribological performance of coconut oil using h-BN. The introduction of h-BN into the coconut oil offered an 84% decrease in COF and 56% in of wear rate [116]. Song and co-workers used polydopamine-decorated boron nitride as nonadditive for epoxy resin with improved tribological properties [117]. Bondarev et al. reported the improvement of the tribological properties of synthetic PAO6 oil using h-BN nanosheets [118]. The addition of h-BN nanosheets to PAO6 oil significantly improved the tribological behavior of the steel tribopair. The COF was decreased to 0.07 when the h-BN addition is 0.01 wt.% and 0.08 when it is 0.1 wt.%. The ball wear rate was reduced from 5.22×10^{-8} mm^3 N^{-1} m^{-1} (for 0.01 wt.% h-BN) to 1.14×10^{-8} mm^3 N^{-1} m^{-1} (for 0.1 wt.% h-BN). The h-BN nanosheets are believed to separate two sliding steel surfaces resulting in the reduction in wear rate. Molecular dynamic simulations indicated that exfoliation and sliding of the h-BN layers under tribological contact do add to the reduction in friction and wear.

4.3.3. Black Phosphorus

Black phosphorus (BP) is a new class of 2D materials that has gained considerable interest in recent years. Besides weak interlayer interaction, BP exhibits other interesting characteristics such as anisotropic lamellar structure, high carrier mobility, tunable bandgap and good thermal stability [119]. Moreover, the high mechanical properties of BP have made it very suitable in obtaining low-friction and low-wear systems; the ideal elastic modulus of zigzag BP nanoribbon is ~65 GPa and the modulus for armchair BP nanoribbons is ~27 GPa [120]. BP is known to be unstable under ambient conditions; few-layer BP surface is prone to oxidize when exposed to visible light, oxygen and water [121]. However, Wu et al. [122] have shown that the ambient degradation of BP favors its lubrication behavior. Using AFM microscopy, they observed a 50% reduction in friction force at the degraded area of the BP flakes as a result of the produced phosphorus oxides during degradation. They suggested that the combination of water molecules and the resultant chemical groups (P–OH bonds) formed on the oxidized surface may be responsible for the friction force reduction of the degraded BP flakes. Several studies have confirmed the anisotropic frictional behavior of single-layer BP nanosheet (phosphorene) using a frictional force microscope (FFM) and simulation models [123,124]. However, Lee at al. recently employed molecular dynamic simulation to systematically analyze the mechanisms of the anisotropic friction occurring at the interfaces of the FFM tip and the phosphorene [125]. They evaluated the influence of experimental parameters such as scan direction, spring stiffness, tip load force and tip size on the frictional behavior. It was suggested that the anisotropic friction depends on the scan direction. Through the analysis of the potential energy profiles, it was shown that the mean friction increases in the armchair direction compared to the zigzag direction. It is worth noting that phosphorene has an uncommon puckered honeycomb structure which impacts it with irregular hexagonal atomic lattice [126,127]. Hence, the scan direction dependence frictional behavior is because the FFM tip had to overcome a larger energy barrier while passing over the puckered honeycomb structure than passing over the bond of phosphorus atoms. So, the tip had to overcome more resistance in the armchair direction. Similarly, the tip's behavior of passing over the bond of phosphorus atom (zigzag direction) and passing over the puckered honeycomb structure (armchair direction) was shown to be the cause of nanoscale and sub-nanoscale stick-slip phenomena in case of the changes in the spring stiffness and tip load size. Furthermore, they showed that a decrease in the FFM tip's diameter resulted in a high-frequency sub-nanoscale stick-slip behavior and reduced nanoscale slip duration. Losi et al. studied the interlayer slipperiness of BP utilizing DFT calculations [128]. It was shown that BP Layers stacked with parallel orientation like an armchair–armchair or zigzag–zigzag orientation is as slippery as the conventional solid lubricants such as MoS_2 and graphite. However, the armchair–zigzag (perpendicular) orientation offered an excellent superlubricity, with one order of magnitude reduction of the shear stress. By observing the electric charge distribution at the interface, the superlubricity behavior was attributed to the strong localization of charges within the perpendicular orientation. Furthermore, Wang and co-workers obtained an extremely low COF value of 0.0006 on an

experiment conducted with ball-on-plate tribometer [119]. They modified BP powder with NaOH via a high-energy-ball-milling (HEBM) technique to obtain BP-OH. Thereafter, an aqueous solution of BP-OH was prepared and its COF was measured in comparison with other lubricants as shown in Figure 12. Interestingly, the robust superlubricity obtained with aqueous BP-OH was seen in an expanded range of additive concentrations, sliding velocities and contact pressures. This outstanding result was attributed to the very low shear resistance of the water layer retained by BP-OH nanosheets. It has been suggested that water molecules are strongly attracted to the BP-OH nanosheet surface because of the formation of hydrogen bonding around the OH headgroups [129]. Wherefore, the dynamically stable layer of water on the surface of the BP-OH nanosheet can offer a very low shear strength due to its remarkable fluidity.

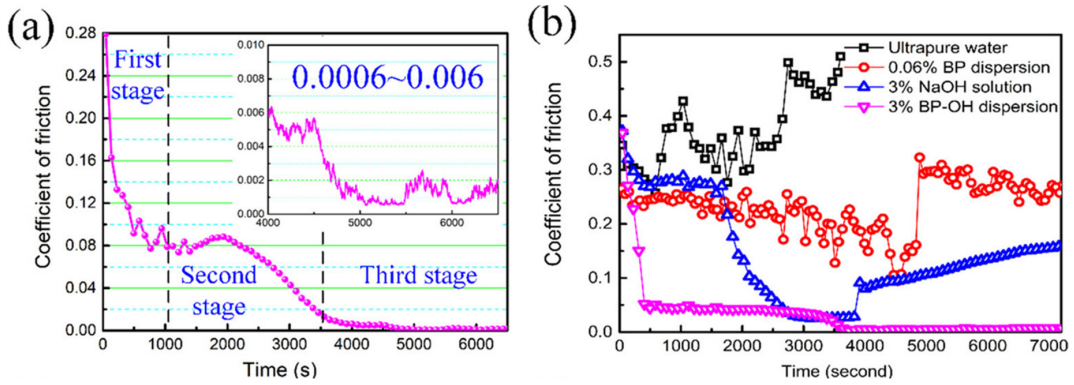

Figure 12. (**a**) Variation in the COF with time using the 7 wt.% BP-OH aqueous solution as the lubricant. The inset is the magnified graph of the COF after the running-in period. (**b**) The comparative plots of the COFs of four different lubricants including ultrapure water, 3% NaOH solution, 0.06% BP Dispersion and 3% BP-OH dispersion. Reproduced with permission from [119]. Copyright 2018 American Chemical Society.

5. Micro-Nano Patterns

It is well known that surface topography could affect friction. Therefore, many researchers around the world are studying the effect of micro/nano textures on friction as well as seeking the optimal textures for different applications. Micro/nano textures are promising in reducing friction mainly due to the following mechanisms. First, micro/nano patterns such as grooves can provide spaces for debris during the friction, therefore reduce the wear caused by debris. Solid debris especially those made of hard materials sandwiched between two friction surfaces can lead to significant mechanical wear. Second, micro/nano patterns can efficiently reduce the actual contact area, therefore also reduce the friction efficiency and wear rate. However, the current understanding of the friction behavior on micro/nano textured surface is not sufficient [130]. One reason is the lack of precise tools to study nanoscale friction. While atomic force microscopy (AFM) is a good platform, an idea spherical AFM probe that has the range from a hundred nanometers to a few microns are missing for this type of study. A recent work by Hu et al. is promising in experimentally studying the tribology in this scale [131].

Figure 13 shows eight different types of micro/nano textures used together with 2D materials that have been demonstrated to be effective in reducing friction.

Figure 13(A1) shows an SEM image of shark-skin type micro grooves structures with WS_2 coatings prepared using electrohydrodynamic atomization (EHDA). The biomimetic microstructure together with WS2 coatings reduced the friction coefficient by 84% and the dropped steel ball wear rate by 86% [132].

Figure 13(A2) shows an SEM image of micro grooves and WS_2 coatings. The combination of micro grooves with 0.679 texture coverage exhibits the lowest friction coefficient and lowest steel ball wear rate, decreasing by ~16% and ~70% [133]. Figure 13(A3) shows an SEM image of textured disk self-assembled with a 3-APS membrane and the inset was the magnification image. The 2D materials

together with micro-hole array textures reduced the friction coefficient by 26% and the wear rate by 39.4% compared with the smooth surface [134]. Figure 13(A4) shows an SEM image of a 363 nm thick GO film atop a silicon micro dimple array, which obtained a friction coefficient five times lower than a non-textured GO film and half the wear rate compared to wear of a non-textured GO film [135]. Figure 13(B1) is the SEM image of WS_2 film textured with a cabbage-like nanocone-array Ni interlayer, which increases the wear life by seven times compared with pure WS2 films and by 1.5 times compared with rough Ni textured WS_2 films [136]. Figure 13(B2) shows an SEM image of MoS_2 on top of AAO membranes that can effectively decrease the friction coefficient by more than 50% [137]. Figure 13(B3) is an SEM image of burnished MoS_2 addition on nano-textured PVD TiAlN coatings. This surface was tested to increase the wear life time of TiAlN coatings against AISI 316 stainless steel by about 40% but not the coefficient of friction [138]. Meng et al. reported that h-BN doesn't reduce friction as well as other 2D materials such as WS_2 and graphite on micro-textured surfaces [139].

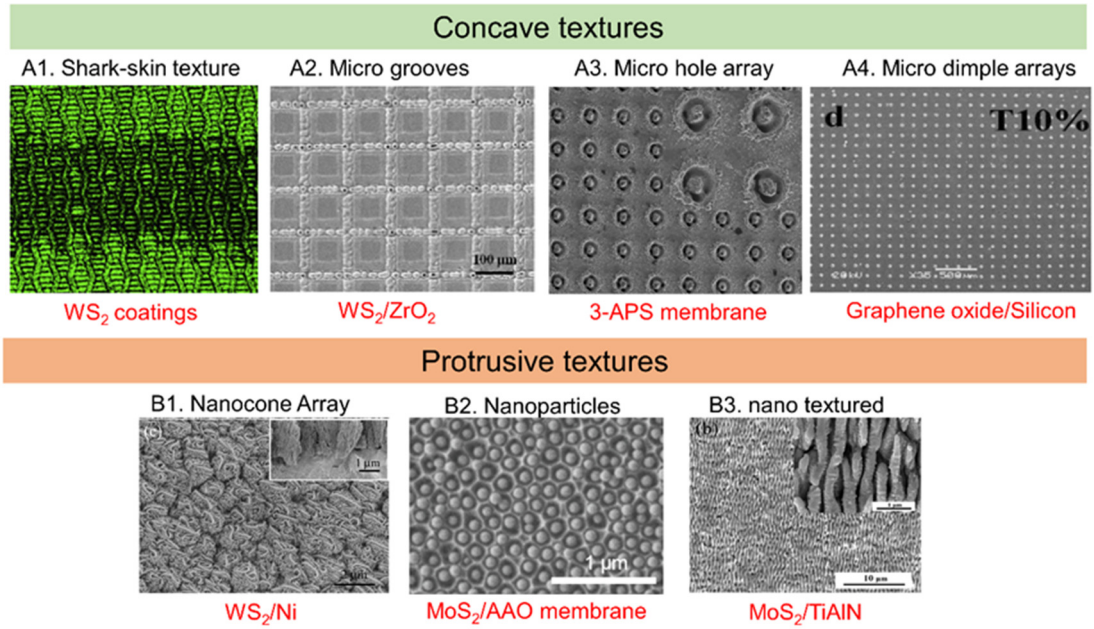

Figure 13. Different types of micro/nano textured surface used with 2D materials for reducing friction coefficients and wear. (**A1**) Shark-skin texture [132]; (**A2**) Linear micro grooves with WS_2 coatings [133]; (**A3**) Micro hole array with 3-APS membranes [134]; (**A4**) Micro dimple arrays of silicon with graphene oxide film on top [135]; (**B1**) Nanocone array of nickel with WS_2 film [136]; (**B2**) Nanoparticles embedded in AAO membranes with MoS_2 films [137]; (**B3**) Nano textured TiAlN with MoS_2 coating [138].

The optimal texture geometries including sizes, shapes, heights depend on the lubrication conditions for tribology applications such as mechanical properties of tribopairs, loading conditions and the environmental parameters [140]. Therefore, optimization of textures lacks a universal guideline and relies on experimental studies for each unique case.

From a manufacturing perspective, producing micro/nano textures on a macro scale and friction parts remains a challenge. Lithography normally occurs on flat and smooth surfaces such as silicon wafers and it will require extra steps to transfer the micropatterns from silicon to metal surface [141]. Laser such as femto-second laser is an emerging method due to its low-cost and the easy of applying it to a broad type of materials regardless of its surface shape and topography. Laser has been used for surface texturing on stainless steel [142], zirconia [143], alumina-titania [144], silicon nitride ceramic [145], etc. However, some challenges remain to be solved including the quality of the produced patterns as well as the lower limits in produced sizes. Other nanofabrication methods such as nanosphere lithography, replica molding, block-polymer are promising in fabricating micro/nano textured surfaces for reducing

frictions in a low-cost fashion, therefore can be applied for macro-scale applications. However, these methods have limited design options.

Now, with the advancement of micro/nano-manufacturing, it is now possible to scale up the micro/nanotexturing on surfaces exposed to friction. The techniques of transfer lithography-produced patterns to metal and polymer surfaces are extremely promising because it takes advantage of the mass-production capability and precise control of pattern geometry of lithography [146].

6. Conclusions and Prospects

Recent developments on the tribological performance of 2D materials as a solid lubricant, composite mixture as well as lubrication nano-additives have been reviewed. However, some challenges are limiting their wide industrial applications. The most common challenge facing 2D materials is the lack of dispersion in oil. Nanomaterials like graphene nanosheets and WS_2 always agglomerate due to high surface ratio and strong van der Waals forces. Such aggregation in lubricants has prevented their broad application. Several scientific techniques ranging from chemical surface modification and alkylation, have been proposed to solve the problem of dispersion [4]. The chemical modification involves the termination of a functional nanoparticle onto the nanosheets or the incorporation of nanoparticles such as α-Fe_2O_3 nanorods, ZnO nanoparticles and Ni nanoparticles in the 2D material [147–149]. This method has proven effective in enhancing the dispersion of the 2D material in oil lubricants. The grafting of alkyl chains on the active sites of reduced graphene oxide (rGO) through amide linkage has been proven to stabilize the dispersion of rGO in oil, resulting in improved tribological performance [150,151]. The addition of surfactants has also been explored for efficient dispersion of graphene in water to enhance tribological behavior, as reported by Liang et al. [152] and Uddin et al. [153]. Besides nanoparticle agglomeration, WS_2 is also limited by its high density. Moreover, despite that MoS_2 exhibits better dispersion, its load-bearing capacity is low when it is employed independently. Therefore, a sizable amount of MoS_2 is usually required to reduce the COF. This might pose a significant challenge to the overall mechanical behavior of the matrix [4]. So, the challenge is achieving very low friction at minimal particle concentration. The common solution is harnessing the synergistic influence of two solid lubricants, particularly graphene, with excellent mechanical properties to compensate for the load-bearing capacity. Moreover, the use of MoS_2 with ceramics to enhance the strength of the lubricants has been reported [4]. Notably, some of these solutions like chemical modification, are limited to laboratory observations. Therefore, further investigation is required to make them feasible and scalable for industrial use.

Furthermore, as humans continue to explore their immediate surroundings (example; the marine environment, deep seas, biomedicals, etc.) and far-away universe such as outer space, the need for excellent lubricants for future machinery keeps arising. For example, the spacecraft has several friction pairs in components like wheel shafts, bearings and sleeves. These tribopairs are expected to perform under severe environmental conditions (that is in the vacuum at about −200 °C–200 °C temperature variation). It means that the use of conventional liquid lubricants is impracticable in such conditions. Moreover, the absence of a heat transfer system, coupled with cosmic irradiation and solar wind, creates an extremely difficult environment for the tribopairs [2]. The presence of friction in tribopairs has been shown to have detrimental effects on the spacecraft and also impede the design procedure [154]. So, to prolong the service life of the spacecraft and ensure reliability, the prospective lubricants must provide superlubricity, adequate hardness, excellent thermal stability and oxidative resistance. Moreover, putting in context other environmental cases where lubricants are required, it becomes necessary that future lubricants should not only possess excellent reduction of friction and wear, they are expected to also exhibit multifunctionality such as anti-fouling, anti-corrosion, anti-thermal, anti-pressure, self-repairing and so on as the demand arises; hence, more research is needed to develop very high-performance multifunctional 2D materials for tribological purposes.

Author Contributions: Draft conception, O.V.P.; writing original draft, P.C.U., M.K., H.H., and O.V.P.; review and editing, P.C.U., M.K., H.H., and O.V.P. All authors have read and agreed to the published version of the manuscript.

Funding: This research received no external funding and the APC was funded by Zhejiang University.

Acknowledgments: This work was supported by the Zhejiang University/University of Illinois at Urbana-Champaign Institute and supervised by Oleksiy Penkov. Mahdi Khadem was supported by the Brain Korea 21 Plus Project in 2020.

Conflicts of Interest: The authors declare no conflict of interest.

References

1. Holmberg, K.; Erdemir, A. Influence of tribology on global energy consumption, costs and emissions. *Friction* **2017**, *5*, 263–284. [CrossRef]
2. Luo, J.; Zhou, X. Superlubricitive engineering—Future industry nearly getting rid of wear and frictional energy consumption. *Friction* **2020**, *8*, 643–665. [CrossRef]
3. Holmberg, K.; Kivikytö-Reponen, P.; Härkisaari, P.; Valtonen, K.; Erdemir, A. Global energy consumption due to friction and wear in the mining industry. *Tribol. Int.* **2017**, *115*, 116–139. [CrossRef]
4. Xiao, H.; Liu, S. 2D nanomaterials as lubricant additive: A review. *Mater. Des.* **2017**, *135*, 319–332. [CrossRef]
5. Penkov, O.; Kim, H.-J.; Kim, H.-J.; Kim, D.-E. Tribology of Graphene: A Review. *Int. J. Precis. Eng. Manuf.* **2014**, *15*, 577–585. [CrossRef]
6. Novoselov, K.S.; Geim, A.K.; Morozov, S.V.; Jiang, D.; Zhang, Y.; Dubonos, S.V.; Grigorieva, I.V.; Firsov, A.A. Electric field effect in atomically thin carbon films. *Science* **2004**, *306*, 666–669. [CrossRef]
7. Geim, A.K.; Novoselov, K.S. The rise of graphene. *Nat. Mater.* **2007**, *6*, 183–191. [CrossRef]
8. Cesano, F.; Scarano, D. Graphene and Other 2D Layered Hybrid Nanomaterial-Based Films: Synthesis, Properties, and Applications. *Coatings* **2018**, *8*, 419. [CrossRef]
9. Tanjil, M.R.-E.; Jeong, Y.; Yin, Z.; Panaccione, W.; Wang, C.M. Angstrom-Scale, Atomically Thin 2D Materials for Corrosion Mitigation and Passivation. *Coatings* **2019**, *9*, 133. [CrossRef]
10. Xia, M. 2D Materials-Coated Plasmonic Structures for SERS Applications. *Coatings* **2018**, *8*, 137. [CrossRef]
11. Dai, W.; Kheireddin, B.; Gao, H.; Kan, Y.; Liang, H. Formation of Anti-Wear Tribofilms via α-ZrP Nanoplatelet as Lubricant Additives. *Lubricants* **2016**, *4*, 28. [CrossRef]
12. Meng, Y.; Su, F.; Chen, Y. Supercritical Fluid Synthesis and Tribological Applications of Silver Nanoparticle-decorated Graphene in Engine Oil Nanofluid. *Sci. Rep.* **2016**, *6*, 31246. [CrossRef] [PubMed]
13. Njiwa, P.; Hadj-Aïssa, A.; Afanasiev, P.; Geantet, C.; Bosselet, F.; Vacher, B.; Belin, M.; Le Mogne, T.; Dassenoy, F. Tribological Properties of New MoS_2 Nanoparticles Prepared by Seed-Assisted Solution Technique. *Tribol. Lett.* **2014**, *55*, 473–481. [CrossRef]
14. Grossiord, C.; Varlot, K.; Martin, J.M.; Le Mogne, T.; Esnouf, C.; Inoue, K. MoS_2 single sheet lubrication by molybdenum dithiocarbamate. *Tribol. Int.* **1998**, *31*, 737–743. [CrossRef]
15. Joly-Pottuz, L.; Dassenoy, F.; Belin, M.; Vacher, B.; Martin, J.M.; Fleischer, N. Ultralow-friction and wear properties of IF-WS_2 under boundary lubrication. *Tribol. Lett.* **2005**, *18*, 477–485. [CrossRef]
16. Liu, L.; Zhou, M.; Li, X.; Jin, L.; Su, G.; Mo, Y.; Li, L.; Zhu, H.; Tian, Y. Research Progress in Application of 2D Materials in Liquid-Phase Lubrication System. *Materials* **2018**, *11*, 1314. [CrossRef] [PubMed]
17. Late, D.J.; Bhat, A.; Rout, C.S. Chapter 2—Fundamentals and Properties of 2D Materials in General and Sensing Applications. In *Fundamentals and Sensing Applications of 2D Materials*; Hywel, M., Rout, C.S., Late, D.J., Eds.; Woodhead Publishing: Sawston/Cambridge, UK, 2019; pp. 5–24.
18. Geim, A.K.; Novoselov, K.S. *Nanoscience and Technology: A Collection of Reviews from Nature Journals*; Rogers, P., Ed.; World Scientific: Singapore, 2010; p. 11.
19. Fiori, G.; Bonaccorso, F.; Iannaccone, G.; Palacios, T.; Neumaier, D.; Seabaugh, A.; Banerjee, S.K.; Colombo, L. Electronics based on two-dimensional materials. *Nat. Nanotechnol.* **2014**, *9*, 768–779. [CrossRef]
20. Choi, J.S.; Kim, J.-S.; Byun, I.-S.; Lee, D.H.; Lee, M.J.; Park, B.H.; Lee, C.; Yoon, D.; Cheong, H.; Lee, K.H.; et al. Friction Anisotropy–Driven Domain Imaging on Exfoliated Monolayer Graphene. *Science* **2011**, *333*, 607–610. [CrossRef]
21. Filleter, T.; McChesney, J.L.; Bostwick, A.; Rotenberg, E.; Emtsev, K.V.; Seyller, T.; Horn, K.; Bennewitz, R. Friction and Dissipation in Epitaxial Graphene Films. *Phys. Rev. Lett.* **2009**, *102*, 086102. [CrossRef]
22. Zhang, S.; Ma, T.; Erdemir, A.; Li, Q. Tribology of two-dimensional materials: From mechanisms to modulating strategies. *Mater. Today* **2019**, *26*, 67–86. [CrossRef]

23. Li, S.; Li, Q.; Carpick, R.W.; Gumbsch, P.; Liu, X.Z.; Ding, X.; Sun, J.; Li, J. The evolving quality of frictional contact with grapheme. *Nature* **2016**, *539*, 541–545. [CrossRef] [PubMed]
24. Mendoza-Sánchez, B.; Gogotsi, Y. Synthesis of Two-Dimensional Materials for Capacitive Energy Storage. *Adv. Mater.* **2016**, *28*, 6104–6135. [CrossRef] [PubMed]
25. Timmerman, M.A.; Xia, R.; Le, P.T.P.; Wang, Y.; ten Elshof, J.E. Metal Oxide Nanosheets as 2D Building Blocks for the Design of Novel Materials. *Chem.-A Eur. J.* **2020**, *26*, 9084–9098. [CrossRef] [PubMed]
26. Zhang, X.; Xie, Y. Recent advances in free-standing two-dimensional crystals with atomic thickness: Design, assembly and transfer strategies. *Chem. Soc. Rev.* **2013**, *42*, 8187–8199. [CrossRef]
27. Koren, E.; Lörtscher, E.; Rawlings, C.; Knoll, A.W.; Duerig, U. Adhesion and friction in mesoscopic graphite contacts. *Science* **2015**, *348*, 679–683. [CrossRef]
28. Liechti, K.M. Understanding friction in layered materials. *Science* **2015**, *348*, 632–633. [CrossRef]
29. Shinjo, K.; Hirano, M. Dynamics of friction: Superlubric State. *Surf. Sci.* **1993**, *283*, 473–478. [CrossRef]
30. Ky, D.L.C.; Bien-Cuong Tran, K.; Le, C.T.; Kim, Y.S.; Chung, K.-H. Friction characteristics of mechanically exfoliated and CVD-grown single-layer MoS_2. *Friction* **2018**, *6*, 395–406. [CrossRef]
31. Lee, C.; Li, Q.; Kalb, W.; Liu, X.-Z.; Berger, H.; Carpick, R.W.; Hone, J. Frictional Characteristics of Atomically Thin Sheets. *Science* **2010**, *328*, 76–80. [CrossRef]
32. Shull, K.R. Contact mechanics and the adhesion of soft solids. *Mater. Sci. Eng. R Rep.* **2002**, *36*, 1–45. [CrossRef]
33. Zhou, X.; Liu, Y.; Hu, X.; Fang, L.; Song, Y.; Liu, D.; Luo, J. Influence of elastic property on the friction between atomic force microscope tips and 2D materials. *Nanotechnology* **2020**, *31*, 285710. [CrossRef] [PubMed]
34. Park, J.Y.; Ogletree, D.F.; Thiel, P.A.; Salmeron, M. Electronic Control of Friction in Silicon pn Junctions. *Science* **2006**, *313*, 186. [CrossRef] [PubMed]
35. Qi, Y.; Park, J.Y.; Hendriksen, B.L.M.; Ogletree, D.F.; Salmeron, M. Electronic contribution to friction on GaAs: An atomic force microscope study. *Phys. Rev. B* **2008**, *77*, 184105. [CrossRef]
36. Berman, D.; Erdemir, A.; Sumant, A.V. Graphene: A new emerging lubricant. *Mater. Today* **2014**, *17*, 31–42. [CrossRef]
37. Hilton, M.R.; Bauer, R.; Didziulis, S.V.; Dugger, M.T.; Keem, J.M.; Scholhamer, J. Structural and tribological studies of MoS_2 solid lubricant films having tailored metal-multilayer nanostructures. *Surf. Coat. Technol.* **1992**, *53*, 13–23. [CrossRef]
38. Ratoi, M.; Niste, V.B.; Walker, J.; Zekonyte, J. Mechanism of Action of WS_2 Lubricant Nanoadditives in High-Pressure Contacts. *Tribol. Lett.* **2013**, *52*, 81–91. [CrossRef]
39. Shi, Q.; Tang, H.; Zhu, H.; Tang, G.; Zhang, K.; Zhang, H.; Li, C. Synthesis and tribological properties of ti-doped $NbSe_2$ nanoparticles. *Chalcogenide Lett.* **2014**, *11*, 199–207.
40. Parvez, K. Chapter 1—Two-Dimensional Nanomaterials: Crystal Structure and Synthesis. In *Biomedical Applications of Graphene and 2D Nanomaterials*; Nurunnabi, M., McCarthy, J.R., Eds.; Elsevier: Amsterdam, The Netherlands, 2019; pp. 1–25.
41. Yi, M.; Shen, Z. A review on mechanical exfoliation for the scalable production of graphene. *J. Mater. Chem. A* **2015**, *3*, 11700–11715. [CrossRef]
42. Novoselov, K.S.; Jiang, D.; Schedin, F.; Booth, T.J.; Khotkevich, V.V.; Morozov, S.V.; Geim, A.K. Two-dimensional atomic crystals. *Proc. Natl. Acad. Sci. USA* **2005**, *102*, 10451–10453. [CrossRef]
43. Li, H.; Wu, J.; Yin, Z.; Zhang, H. Preparation and Applications of Mechanically Exfoliated Single-Layer and Multilayer MoS_2 and WSe_2 Nanosheets. *Acc. Chem. Res.* **2014**, *47*, 1067–1075. [CrossRef]
44. Li, H.; Lu, G.; Wang, Y.; Yin, Z.; Cong, C.; He, Q.; Wang, L.; Ding, F.; Yu, T.; Zhang, H. Mechanical Exfoliation and Characterization of Single- and Few-Layer Nanosheets of WSe_2, TaS_2, and $TaSe_2$. *Small* **2013**, *9*, 1974–1981. [CrossRef] [PubMed]
45. Late, D.J.; Doneux, T.; Bougouma, M. Single-layer $MoSe_2$ based NH_3 gas sensor. *Appl. Phys. Lett.* **2014**, *105*, 233103. [CrossRef]
46. Shmavonyan, G.S.; Sevoyan, G.; Aroutiounian, V.M. Enlarging the surface area of monolayer graphene synthesized by mechanical exfoliation. *Armen. J. Phys.* **2013**, *6*, 1–6.
47. Peng, Y.; Wang, Z.; Zou, K. Friction and Wear Properties of Different Types of Graphene Nanosheets as Effective Solid Lubricants. *Langmuir* **2015**, *31*, 7782–7791. [CrossRef]
48. Zhang, Y.; Small, J.P.; Pontius, W.V.; Kim, P. Fabrication and electric-field-dependent transport measurements of mesoscopic graphite devices. *Appl. Phys. Lett.* **2005**, *86*, 073104. [CrossRef]

49. Lee, J.H.; Park, S.J.; Choi, J.W. Electrical Property of Graphene and Its Application to Electrochemical Biosensing. *Nanomaterials* **2019**, *9*, 297. [CrossRef]
50. Hernandez, Y.; Nicolosi, V.; Lotya, M.; Blighe, F.M.; Sun, Z.; De, S.; McGovern, I.T.; Holland, B.; Byrne, M.; Gun'Ko, Y.K.; et al. High-yield production of graphene by liquid-phase exfoliation of graphite. *Nat. Nanotechnol.* **2008**, *3*, 563–568. [CrossRef]
51. Coleman, J.N.; Lotya, M.; O'Neill, A.; Bergin, S.D.; King, P.J.; Khan, U.; Young, K.; Gaucher, A.; De, S.; Smith, R.J.; et al. Two-dimensional nanosheets produced by liquid exfoliation of layered materials. *Science* **2011**, *331*, 568–571. [CrossRef]
52. Singh, V.; Joung, D.; Zhai, L.; Das, S.; Khondaker, S.I.; Seal, S. Graphene based materials: Past, present and future. *Prog. Mater. Sci.* **2011**, *56*, 1178–1271. [CrossRef]
53. Zhang, Y.; Zhang, L.; Zhou, C. Review of Chemical Vapor Deposition of Graphene and Related Applications. *Acc. Chem. Res.* **2013**, *46*, 2329–2339. [CrossRef]
54. Somani, P.R.; Somani, S.P.; Umeno, M. Planer nano-graphenes from camphor by CVD. *Chem. Phys. Lett.* **2006**, *430*, 56–59. [CrossRef]
55. Li, X.; Cai, W.; An, J.; Kim, S.; Nah, J.; Yang, D.; Piner, R.; Velamakanni, A.; Jung, I.; Tutuc, E.; et al. Large-Area Synthesis of High-Quality and Uniform Graphene Films on Copper Foils. *Science* **2009**, *324*, 1312–1314. [CrossRef] [PubMed]
56. Zhan, Y.; Liu, Z.; Najmaei, S.; Ajayan, P.M.; Lou, J. Large-Area Vapor-Phase Growth and Characterization of MoS_2 Atomic Layers on a SiO_2 Substrate. *Small* **2012**, *8*, 966–971. [CrossRef]
57. Li, X.; Cai, W.; Colombo, L.; Ruoff, R.S. Evolution of Graphene Growth on Ni and Cu by Carbon Isotope Labeling. *Nano Lett.* **2009**, *9*, 4268–4272. [CrossRef]
58. Singh, R.; Kumar, D.; Tripathi, C.C. Graphene: Potential material for nanoelectric applications, India. *J. Pure Appl. Phys.* **2015**, *53*, 501–513.
59. Jia, G.; Plentz, J.; Dellith, J.; Dellith, A.; Wahyuono, R.A.; Andrae, G. Large Area Graphene Deposition on Hydrophobic Surfaces, Flexible Textiles, Glass Fibers and 3D Structures. *Coatings* **2019**, *9*, 183. [CrossRef]
60. Lee, C.; Wei, X.; Kysar, J.W.; Hone, J. Measurement of the Elastic Properties and Intrinsic Strength of Monolayer Graphene. *Science* **2008**, *321*, 385–388. [CrossRef]
61. Zhu, C.; Yan, Y.; Wang, F.; Cui, J.; Zhao, S.; Gao, A.; Zhang, G. Facile fabrication of long-chain alkyl functionalized ultrafine reduced graphene oxide nanocomposites for enhanced tribological performance. *RSC Adv.* **2019**, *9*, 7324–7333. [CrossRef]
62. Bunch, J.S.; Verbridge, S.S.; Alden, J.S.; van der Zande, A.M.; Parpia, J.M.; Craighead, H.G.; McEuen, P.L. Impermeable Atomic Membranes from Graphene Sheets. *Nano Lett.* **2008**, *8*, 2458–2462. [CrossRef]
63. Blau, P.J. Four great challenges confronting our understanding and modeling of sliding friction**Research sponsored by the U.S. Department of Energy, Assistant Secretary for Energy Efficiency and Renewable Energy, office of Transportation Technologies, as part of the Heavy Vehicle Propulsion System Materials Program, under contract DE-AC05-960R22464 with Lockheed Martin Energy Research Corporation. In *Tribology Series*; Dowson, D., Taylor, C.M., Childs, T.H.C., Dalmaz, G., Berthier, Y., Flamand, L., Georges, J.M., Lubrecht, A.A., Eds.; Elsevier: Amsterdam, The Netherlands, 1998; pp. 117–128.
64. Shakhvorostov, D.; Pöhlmann, K.; Scherge, M. An energetic approach to friction, wear and temperature. *Wear* **2004**, *257*, 124–130. [CrossRef]
65. Blau, P.J. On the nature of running-in. *Tribol. Int.* **2005**, *38*, 1007–1012. [CrossRef]
66. Zhao, S.; Shi, S.; Xia, K.; Wang, T.; Chai, M.; Zhang, Y.; Qu, C.; Zheng, Q. Scratching of Graphene-Coated Cu Substrates Leads to Hardened Cu Interfaces with Enhanced Lubricity. *ACS Appl. Nano Mater.* **2020**, *3*, 1992–1998. [CrossRef]
67. Yao, Q.; Qi, Y.; Zhang, J.; Zhang, S.; Zhao, P.; Wang, H.; Feng, X.-Q.; Li, Q. Impacts of the substrate stiffness on the anti-wear performance of grapheme. *AIP Adv.* **2019**, *9*, 075317. [CrossRef]
68. Savage, R.H. Graphite Lubrication. *J. Appl. Phys.* **1948**, *19*, 1–10. [CrossRef]
69. Lancaster, J.K.; Pritchard, J.R. The influence of environment and pressure on the transition to dusting wear of graphite. *J. Phys. D Appl. Phys.* **1981**, *14*, 747–762. [CrossRef]
70. Nair, R.R.; Wu, H.A.; Jayaram, P.N.; Grigorieva, I.V.; Geim, A.K. Unimpeded Permeation of Water through Helium-Leak–Tight Graphene-Based Membranes. *Science* **2012**, *335*, 442–444. [CrossRef] [PubMed]

71. Tocci, G.; Joly, L.; Michaelides, A. Friction of Water on Graphene and Hexagonal Boron Nitride from Ab Initio Methods: Very Different Slippage Despite Very Similar Interface Structures. *Nano Lett.* **2014**, *14*, 6872–6877. [CrossRef]
72. Chen, W.; Foster, A.S.; Alava, M.J.; Laurson, L. Stick-Slip Control in Nanoscale Boundary Lubrication by Surface Wettability. *Phys. Rev. Lett.* **2015**, *114*, 095502. [CrossRef]
73. Lin, H.; Rauf, A.; Severin, N.; Sokolov, I.M.; Rabe, J.P. Influence of interface hydration on sliding of graphene and molybdenum-disulfide single-layers. *J. Colloid Interface Sci.* **2019**, *540*, 142–147. [CrossRef]
74. Lee, H.; Ko, J.-H.; Choi, J.S.; Hwang, J.H.; Kim, Y.-H.; Salmeron, M.; Park, J.Y. Enhancement of Friction by Water Intercalated between Graphene and Mica. *J. Phys. Chem. Lett.* **2017**, *8*, 3482–3487. [CrossRef]
75. Xu, K.; Cao, P.; Heath, J.R. Graphene Visualizes the First Water Adlayers on Mica at Ambient Conditions. *Science* **2010**, *329*, 1188–1191. [CrossRef]
76. Severin, N.; Lange, P.; Sokolov, I.M.; Rabe, J.P. Reversible Dewetting of a Molecularly Thin Fluid Water Film in a Soft Graphene–Mica Slit Pore. *Nano Lett.* **2012**, *12*, 774–779. [CrossRef]
77. Li, Q.; Song, J.; Besenbacher, F.; Dong, M. Two-Dimensional Material Confined Water. *Acc. Chem. Res.* **2015**, *48*, 119–127. [CrossRef]
78. Lee, M.J.; Choi, J.S.; Kim, J.-S.; Byun, I.-S.; Lee, D.H.; Ryu, S.; Lee, C.; Park, B.H. Characteristics and effects of diffused water between graphene and a SiO_2 substrate. *Nano Res.* **2012**, *5*, 710–717. [CrossRef]
79. Dou, X.; Koltonow, A.R.; He, X.; Jang, H.D.; Wang, Q.; Chung, Y.-W.; Huang, J. Self-dispersed crumpled graphene balls in oil for friction and wear reduction. *Proc. Natl. Acad. Sci. USA* **2016**, *113*, 1528–1533. [CrossRef]
80. Mutyala, K.C.; Wu, Y.A.; Erdemir, A.; Sumant, A.V. Graphene—MoS_2 ensembles to reduce friction and wear in DLC-Steel contacts. *Carbon* **2019**, *146*, 524–527. [CrossRef]
81. Berman, D.; Erdemir, A.; Sumant, A.V. Reduced wear and friction enabled by graphene layers on sliding steel surfaces in dry nitrogen. *Carbon* **2013**, *59*, 167–175. [CrossRef]
82. Qi, W.; Huang, P.; Chen, X.; Jin, J.; Luo, J. Achieving controllable friction of ultrafine-grained graphite HPG510 by tailoring the interfacial nanostructures. *Appl. Surf. Sci.* **2020**, *512*, 145731. [CrossRef]
83. Han, J.-S.; Choi, J.-Y.; Yoo, M.; Lee, C.-S. Synthesis, Dispersion, and Tribological Performance of Alkyl-functionalized Graphene Oxide as an Oil Lubricant Additive and Synergistic Interaction with IF-WS_2. *Bull. Korean Chem. Soc.* **2020**, *41*, 518–529. [CrossRef]
84. Berman, D.; Mutyala, K.C.; Srinivasan, S.; Sankaranarayanan, S.K.R.S.; Erdemir, A.; Shevchenko, E.V.; Sumant, A.V. Iron-Nanoparticle Driven Tribochemistry Leading to Superlubric Sliding Interfaces. *Adv. Mater. Interfaces* **2019**, *6*, 1901416. [CrossRef]
85. Uzoma, P.C.; Liu, F.; Xu, L.; Zhang, Z.; Han, E.-H.; Ke, W.; Arukalam, I.O. Superhydrophobicity, conductivity and anticorrosion of robust siloxane-acrylic coatings modified with graphene nanosheets. *Prog. Org. Coat.* **2019**, *127*, 239–251. [CrossRef]
86. Ge, X.; Li, J.; Wang, H.; Zhang, C.; Liu, Y.; Luo, J. Macroscale superlubricity under extreme pressure enabled by the combination of graphene-oxide nanosheets with ionic liquid. *Carbon* **2019**, *151*, 76–83. [CrossRef]
87. Dev Srivyas, P.; Charoo, M.S. Tribological characterization of hybrid aluminum composite under boundary lubricating sliding conditions. *Mater. Today: Proc.* **2020**, *26*, 492–500. [CrossRef]
88. Mohseni Taromsari, S.; Salari, M.; Bagheri, R.; Faghihi Sani, M.A. Optimizing tribological, tensile & in-vitro biofunctional properties of UHMWPE based nanocomposites with simultaneous incorporation of graphene nanoplatelets (GNP) & hydroxyapatite (HAp) via a facile approach for biomedical applications. *Compos. Part B Eng.* **2019**, *175*, 107181.
89. Papageorgiou, D.G.; Kinloch, I.A.; Young, R.J. Mechanical properties of graphene and graphene-based nanocomposites. *Prog. Mater. Sci.* **2017**, *90*, 75–127. [CrossRef]
90. Tai, Z.; Chen, Y.; An, Y.; Yan, X.; Xue, Q. Tribological Behavior of UHMWPE Reinforced with Graphene Oxide Nanosheets. *Tribol. Lett.* **2012**, *46*, 55–63. [CrossRef]
91. Das, B.; Eswar Prasad, K.; Ramamurty, U.; Rao, C.N.R. Nano-indentation studies on polymer matrix composites reinforced by few-layer graphene. *Nanotechnology* **2009**, *20*, 125705. [CrossRef]
92. Castellanos-Gomez, A.; Poot, M.; Steele, G.A.; van der Zant, H.S.J.; Agraït, N.; Rubio-Bollinger, G. Elastic Properties of Freely Suspended MoS_2 Nanosheets. *Adv. Mater.* **2012**, *24*, 772–775. [CrossRef]
93. Bertolazzi, S.; Brivio, J.; Kis, A. Stretching and Breaking of Ultrathin MoS_2. *ACS Nano* **2011**, *5*, 9703–9709. [CrossRef]

94. Serpini, E.; Rota, A.; Valeri, S.; Ukraintsev, E.; Rezek, B.; Polcar, T.; Nicolini, P. Nanoscale frictional properties of ordered and disordered MoS_2. *Tribol. Int.* **2019**, *136*, 67–74. [CrossRef]
95. Bui, H.S. Influence of Different Environement on the Tribological Behavior of Molybdenum Disulfide MoS_2. *Int. J. Innov. Sci. Res. Technol.* **2020**, *5*, 478–481.
96. Clauss, F.J. Chapter 4—Molybdenum Disulfide. In *Solid Lubricants and Self-Lubricating Solids*; Clauss, F.J., Ed.; Academic Press: Cambridge, MA, USA, 1972; pp. 75–112.
97. Cao, X.A.; Gan, X.; Lang, H.; Yu, K.; Ding, S.; Peng, Y.; Yi, W. Anisotropic nanofriction on MoS_2 with different thicknesses. *Tribol. Int.* **2019**, *134*, 308–316. [CrossRef]
98. Chhowalla, M.; Shin, H.S.; Eda, G.; Li, L.-J.; Loh, K.P.; Zhang, H. The chemistry of two-dimensional layered transition metal dichalcogenide nanosheets. *Nat. Chem.* **2013**, *5*, 263–275. [CrossRef] [PubMed]
99. Acikgoz, O.; Baykara, M.Z. Speed dependence of friction on single-layer and bulk MoS_2 measured by atomic force microscopy. *Appl. Phys. Lett.* **2020**, *116*, 071603. [CrossRef]
100. Wu, P.-R.; Li, W.; Ge, T.; Feng, Y.-M.; Liu, Z.; Cheng, Z.-L. Preparation and tribological properties of chemically decorated MoS_2 nanosheets with oleic diethanolamide. *Lubr. Sci.* **2019**, *31*, 41–50.
101. Li, Y.; Xie, M.; Sun, Q.; Xu, X.; Fan, X.; Zhang, G.; Li, H.; Zhu, M. The effect of atmosphere on the tribological behavior of magnetron sputtered MoS_2 coatings. *Surf. Coat. Technol.* **2019**, *378*, 125081. [CrossRef]
102. Chen, B.; Zhang, M.; Li, X.; Dong, Z.; Jia, Y.; Li, C. Tribological properties of epoxy-based self-lubricating composite coating enhanced by 2D/2D h-BN/ MoS_2 hybrid. *Prog. Org. Coat.* **2020**, *147*, 105767. [CrossRef]
103. Yu, G.; Gong, Z.; Jiang, B.; Wang, D.; Bai, C.; Zhang, J. Superlubricity for hydrogenated diamond like carbon induced by thin MoS_2 and DLC layer in moist air. *Diam. Relat. Mater.* **2020**, *102*, 107668. [CrossRef]
104. Jiang, Z.; Zhang, Y.; Yang, G.; Yang, K.; Zhang, S.; Yu, L.; Zhang, P. Tribological Properties of Oleylamine-Modified Ultrathin WS_2 Nanosheets as the Additive in Polyalpha Olefin Over a Wide Temperature Range. *Tribol. Lett.* **2016**, *61*, 24. [CrossRef]
105. Evaristo, M.; Fernandes, F.; Cavaleiro, A. Room and High Temperature Tribological Behaviour of W-DLC Coatings Produced by DCMS and Hybrid DCMS-HiPIMS Configuration. *Coatings* **2020**, *10*, 319. [CrossRef]
106. Aldana, P.U.; Vacher, B.; Le Mogne, T.; Belin, M.; Thiebaut, B.; Dassenoy, F. Action Mechanism of WS_2 Nanoparticles with ZDDP Additive in Boundary Lubrication Regime. *Tribol. Lett.* **2014**, *56*, 249–258. [CrossRef]
107. An, V.; Irtegov, Y.; de Izarra, C. Study of Tribological Properties of Nanolamellar WS_2 and MoS_2 as Additives to Lubricants. *J. Nanomater.* **2014**, *2014*, 1–8.
108. Ma, L.; Liu, Z.; Cheng, Z.-L. Scalable exfoliation and friction performance of few-layered WS_2 nanosheets by microwave-assisted liquid-phase sonication. *Ceram. Int.* **2020**, *46*, 3786–3792. [CrossRef]
109. Hu, N.; Zhang, X.; Wang, X.; Wu, N.; Wang, S. Study on Tribological Properties and Mechanisms of Different Morphology WS_2 as Lubricant Additives. *Materials* **2020**, *13*, 1522. [CrossRef] [PubMed]
110. Xu, S.; Sun, J.; Weng, L.; Hua, Y.; Liu, W.; Neville, A.; Hu, M.; Gao, X. In-situ friction and wear responses of WS_2 films to space environment: Vacuum and atomic oxygen. *Appl. Surf. Sci.* **2018**, *447*, 368–373. [CrossRef]
111. Fu, Y.; Jiang, D.; Wang, D.; Gao, X.; Hu, M.; Yang, W. Tribological Performance of MoS_2- WS_2 Composite Film under the Atomic Oxygen Irradiation Conditions. *Materials* **2020**, *13*, 1407. [CrossRef]
112. Gao, X.; Fu, Y.; Jiang, D.; Wang, D.; Xu, S.; Liu, W.; Weng, L.; Yang, J.; Sun, J.; Hu, M. Constructing WS_2/MoS_2 nano-scale multilayer film and understanding its positive response to space environment. *Surf. Coat. Technol.* **2018**, *353*, 8–17. [CrossRef]
113. He, X.; Xiao, H.; Choi, H.; Díaz, A.; Mosby, B.; Clearfield, A.; Liang, H. α-Zirconium phosphate nanoplatelets as lubricant additives. *Colloids Surf. A Physicochem. Eng. Asp.* **2014**, *452*, 32–38. [CrossRef]
114. Bondarev, A.V.; Kovalskii, A.M.; Firestein, K.L.; Loginov, P.A.; Sidorenko, D.A.; Shvindina, N.V.; Sukhorukova, I.V.; Shtansky, D.V. Hollow spherical and nanosheet-base BN nanoparticles as perspective additives to oil lubricants: Correlation between large-scale friction behavior and in situ TEM compression testing. *Ceram. Int.* **2018**, *44*, 6801–6809. [CrossRef]
115. Ma, Z.-S.; Ding, H.-L.; Liu, Z.; Cheng, Z.-L. Preparation and tribological properties of hydrothermally exfoliated ultrathin hexagonal boron nitride nanosheets (BNNSs) in mixed NaOH/KOH solution. *J. Alloy. Compd.* **2019**, *784*, 807–815. [CrossRef]
116. Sagbas, B. Tribological performance of PEEK with green lubricant enhanced by nano hexagonal boron nitride powder. *Ind. Lubr. Tribol.* **2020**, *72*, 203–210. [CrossRef]

117. Song, J.; Dai, Z.D.; Li, J.Y.; Tong, X.; Zhao, H.C. Polydopamine-decorated boron nitride as nano-reinforcing fillers for epoxy resin with enhanced thermomechanical and tribological properties. *Mater. Res. Express* **2018**, *5*, 075029. [CrossRef]
118. Bondarev, A.V.; Fraile, A.; Polcar, T.; Shtansky, D.V. Mechanisms of friction and wear reduction by h-BN nanosheet and spherical W nanoparticle additives to base oil: Experimental study and molecular dynamics simulation. *Tribol. Int.* **2020**, *151*, 106493. [CrossRef]
119. Wang, W.; Xie, G.; Luo, J. Superlubricity of Black Phosphorus as Lubricant Additive. *ACS Appl. Mater. Interfaces* **2018**, *10*, 43203–43210. [CrossRef] [PubMed]
120. Chen, H.; Huang, P.; Guo, D.; Xie, G. Anisotropic Mechanical Properties of Black Phosphorus Nanoribbons. *J. Phys. Chem. C* **2016**, *120*, 29491–29497. [CrossRef]
121. Zhou, Q.; Chen, Q.; Tong, Y.; Wang, J. Light-Induced Ambient Degradation of Few-Layer Black Phosphorus: Mechanism and Protection. *Angew. Chem. Int. Ed.* **2016**, *55*, 11437–11441. [CrossRef]
122. Wu, S.; He, F.; Xie, G.; Bian, Z.; Luo, J.; Wen, S. Black Phosphorus: Degradation Favors Lubrication. *Nano Lett.* **2018**, *18*, 5618–5627. [CrossRef] [PubMed]
123. Cui, Z.; Xie, G.; He, F.; Wang, W.; Guo, D.; Wang, W. Atomic-Scale Friction of Black Phosphorus: Effect of Thickness and Anisotropic Behavior. *Adv. Mater. Interfaces* **2017**, *4*, 1700998. [CrossRef]
124. Bai, L.; Liu, B.; Srikanth, N.; Tian, Y.; Zhou, K. Nano-friction behavior of phosphorene. *Nanotechnology* **2017**, *28*, 355704. [CrossRef]
125. Lee, H.G.; Yoon, H.M.; Lee, J.S. Anisotropic nanoscale and sub-nanoscale friction behaviors between phosphorene and silicon tip. *Appl. Surf. Sci.* **2019**, *481*, 1573–1584. [CrossRef]
126. Sha, Z.-D.; Pei, Q.-X.; Ding, Z.; Jiang, J.-W.; Zhang, Y.-W. Mechanical properties and fracture behavior of single-layer phosphorene at finite temperatures. *J. Phys. D Appl. Phys.* **2015**, *48*, 395303. [CrossRef]
127. Jiang, J.-W.; Park, H.S. Mechanical properties of single-layer black phosphorus. *J. Phys. D Appl. Phys.* **2014**, *47*, 385304. [CrossRef]
128. Losi, G.; Restuccia, P.; Righi, M.C. Superlubricity in phosphorene identified by means of ab initio calculations. *2D Mater.* **2020**, *7*, 025033. [CrossRef]
129. Ishikawa, Y.; Hiratsuka, K.-I.; Sasada, T. Role of water in the lubrication of hydrogel. *Wear* **2006**, *261*, 500–504. [CrossRef]
130. Han, J.; Sun, J.P.; Xu, S.; Song, D.; Han, Y.; Zhu, H.; Fang, L. Tuning the Friction of Silicon Surfaces Using Nanopatterns at the Nanoscale. *Coatings* **2018**, *8*, 7. [CrossRef]
131. Hu, H.; Shi, B.; Breslin, C.M.; Gignac, L.; Peng, Y. A Sub-Micron Spherical Atomic Force Microscopic Tip for Surface Measurements. *Langmuir* **2020**, *36*, 7861–7867. [CrossRef]
132. Li, X.; Deng, J.; Yue, H.; Ge, D.; Zou, X. Wear performance of electrohydrodynamically atomized WS_2 coatings deposited on biomimetic shark-skin textured surfaces. *Tribol. Int.* **2019**, *134*, 240–251. [CrossRef]
133. Li, X.; Deng, J.; Zhang, L.; Liu, Y.; Yue, H.; Duan, R.; Ge, D. Effect of surface textures and electrohydrodynamically atomized WS_2 films on the friction and wear properties of ZrO_2 coatings. *Ceram. Int.* **2019**, *45*, 1020–1030. [CrossRef]
134. Li, X.; Liu, Q.; Dong, G. Self-assembly membrane on textured surface for enhancing lubricity of graphene oxide nano-additive. *Appl. Surf. Sci.* **2020**, *505*, 144572. [CrossRef]
135. Jia, X.; Wang, C.; Xiong, G.; Zhu, F. Surface micro-texturing design for improving tribological behaviour of graphene oxide thin films. *Bull. Mater. Sci.* **2019**, *42*, 236. [CrossRef]
136. Wang, D.; Hu, M.; Jiang, D.; Gao, X.; Fu, Y.; Sun, J.; Weng, L. Cabbage-like WS_2/Ni bilayer thin film for improved tribological property. *Surf. Coat. Technol.* **2019**, *358*, 50–56. [CrossRef]
137. Sekiguchi, K.; Katsumata, K.-I.; Segawa, H.; Nakanishi, T.; Yasumori, A. Fabrication of a Silica–Silica Nanoparticle Monolayer Array Nanocomposite Film on an Anodic Aluminum Oxide Substrate and Its Optical and Tribological Properties. *ACS Appl. Mater. Interfaces* **2020**, *12*, 27672–27681. [CrossRef] [PubMed]
138. Zhang, K.; Deng, J.; Lei, S.; Yu, X. Effect of micro/nano-textures and burnished MoS_2 addition on the tribological properties of PVD TiAlN coatings against AISI 316 stainless steel. *Surf. Coat. Technol.* **2016**, *291*, 382–395. [CrossRef]
139. Meng, R.; Deng, J.; Duan, R.; Liu, Y.; Zhang, G. Modifying tribological performances of AISI 316 stainless steel surfaces by laser surface texturing and various solid lubricants. *Opt. Laser Technol.* **2019**, *109*, 401–411. [CrossRef]

140. Mao, B.; Siddaiah, A.; Liao, Y.; Menezes, P.L. Laser surface texturing and related techniques for enhancing tribological performance of engineering materials: A review. *J. Manuf. Process.* **2020**, *53*, 153–173. [CrossRef]
141. Cannon, A.H.; King, W.P. Casting metal microstructures from a flexible and reusable mold. *J. Micromech. Microeng.* **2009**, *19*, 095016. [CrossRef]
142. Wang, Z.; Zhao, Q.Z.; Wang, C.W.; Zhang, Y. Modulation of dry tribological property of stainless steel by femtosecond laser surface texturing. *Appl. Phys. A-Mater.* **2015**, *119*, 1155–1163. [CrossRef]
143. Yilbas, B.S. Laser treatment of zirconia surface for improved surface hydrophobicity. *J. Alloy. Compd.* **2015**, *625*, 208–215. [CrossRef]
144. Wahab, J.A.; Ghazali, M.J.; Sajuri, Z.; Otsuka, Y.; Jayaprakash, M.; Nakamura, S.; Baharin, A.F.S. Effects of micro-grooves on tribological behaviour of plasma-sprayed alumina-13%titania coatings. *Ceram. Int.* **2017**, *43*, 6410–6416. [CrossRef]
145. Xing, Y.Q.; Deng, J.X.; Wu, Z.; Cheng, H.W. Effect of regular surface textures generated by laser on tribological behavior of Si3N4/TiC ceramic. *Appl. Surf. Sci.* **2013**, *265*, 823–832. [CrossRef]
146. Ramesh, A.; Akram, W.; Mishra, S.P.; Cannon, A.H.; Polycarpou, A.A.; King, W.P. Friction characteristics of microtextured surfaces under mixed and hydrodynamic lubrication. *Tribol. Int.* **2013**, *57*, 170–176. [CrossRef]
147. Song, H.-J.; Jia, X.-H.; Li, N.; Yang, X.-F.; Tang, H. Synthesis of α-Fe_2O_3 nanorod/graphene oxide composites and their tribological properties. *J. Mater. Chem.* **2012**, *22*, 895–902. [CrossRef]
148. Zhou, Q.; Huang, J.; Wang, J.; Yang, Z.; Liu, S.; Wang, Z.; Yang, S. Preparation of a reduced graphene oxide/zirconia nanocomposite and its application as a novel lubricant oil additive. *RSC Adv.* **2015**, *5*, 91802–91812. [CrossRef]
149. Meng, Y.; Su, F.; Chen, Y. A Novel Nanomaterial of Graphene Oxide Dotted with Ni Nanoparticles Produced by Supercritical CO_2-Assisted Deposition for Reducing Friction and Wear. *ACS Appl. Mater. Interfaces* **2015**, *7*, 11604–11612. [CrossRef] [PubMed]
150. Mungse, H.P.; Khatri, O.P. Chemically Functionalized Reduced Graphene Oxide as a Novel Material for Reduction of Friction and Wear. *J. Phys. Chem. C* **2014**, *118*, 14394–14402. [CrossRef]
151. Zhang, W.; Zhou, M.; Zhu, H.; Tian, Y.; Wang, K.; Wei, J.; Ji, F.; Li, X.; Li, Z.; Zhang, P.; et al. Tribological properties of oleic acid-modified graphene as lubricant oil additives. *J. Phys. D Appl. Phys.* **2011**, *44*, 205303. [CrossRef]
152. Liang, S.; Shen, Z.; Yi, M.; Liu, L.; Zhang, X.; Ma, S. In-situ exfoliated graphene for high-performance water-based lubricants. *Carbon* **2016**, *96*, 1181–1190. [CrossRef]
153. Uddin, M.E.; Kuila, T.; Nayak, G.C.; Kim, N.H.; Ku, B.-C.; Lee, J.H. Effects of various surfactants on the dispersion stability and electrical conductivity of surface modified graphene. *J. Alloy. Compd.* **2013**, *562*, 134–142. [CrossRef]
154. Lu, S.; Qi, X.; Hu, Y.; Li, B.; Zhang, J. Deployment Dynamics of Large Space Antenna and Supporting Arms. *IEEE Access* **2019**, *7*, 69922–69935. [CrossRef]